Channel Prediction with Location Uncertainty for Ad-Hoc Networks

N.B. When citing this work, cite the original published paper.

(article starts on next page)

Channel Prediction with Location Uncertainty for Ad-Hoc Networks

Markus Fröhle, *Student Member, IEEE,* Themistoklis Charalambous, *Member, IEEE,* Ido Nevat, and Henk Wymeersch *Member, IEEE*

Abstract—**Multi-agent systems (MAS) rely on positioning technologies to determine their physical location, and on wireless communication technologies to exchange information. Both positioning and communication are affected by uncertainties, which should be accounted for. This paper considers an agent placement problem to optimize end-to-end communication quality in a MAS, in the presence of uncertainties. Using Gaussian processes (GPs), operating on the input space of location distributions, we are able to model, learn, and predict the wireless channel. Predictions, in the form of distributions, are fed into the communication optimization problems. This approach inherently avoids regions of the workspace with high position uncertainty and leads to better average communication performance. We illustrate the benefits of our approach via extensive simulations, based on real wireless channel measurements. Finally, we demonstrate the improved channel learning and prediction performance, as well as the increased robustness in agent placement.**

Index Terms—**Ad-hoc networks, bit error rate, channel prediction, Gaussian processes, multi-agent systems**

I. INTRODUCTION

MOBILE autonomous multi-agent systems (MAS) need to communicate and coordinate with each other, as well as interact with the environment they operate in [1]. Such systems employ the wireless medium for communication and localization. For mission planning and its successful execution, it is imperative to have accurate prediction models of the wireless channel, thus allowing to determine the channel quality and prediction accuracy of the future locations of agents within the environment. MAS come in two forms: infrastructure-based MAS, where the agents' communication is only via a fixed infrastructure, and cooperative MAS, where agents communicate over the wireless channel in an ad-hoc manner. Examples of infrastructure-based MAS include

M. Fröhle and H. Wymeersch are with the Department of Electrical Engineering (former name: Department of Signals and Systems), Chalmers University of Technology, 412 96 Gothenburg, Sweden (e-mail: {frohle, henkw}@chalmers.se).

T. Charalambous was with the Department of Signals and Systems, Chalmers University of Technology, 412 96 Gothenburg, Sweden. Currently, he is with the Department of Electrical Engineering and Automation, Aalto University, 02150 Espoo, Finland (e-mail: themistoklis.charalambous@aalto.fi).

I. Nevat is with TUMCREATE, 138602, Singapore (e-mail: idonevat@gmail.com).

maintaining connectivity with a base station [2], proactive caching of data for mobile users [3], [4], and autonomous cars communicating with an intersection coordinator (vehicle-to-infrastructure communication) [5]–[7]. In cooperative MAS, the channel predictor needs to consider mobility of both link endpoints. Examples of cooperative MAS include groups of robots for monitoring [8], search-and-rescue scenarios [9], and autonomous cars cooperating on sensor data from the environment [10], as well as their throughput maximization at an intersection (vehicle-to-vehicle communication) [11]. Furthermore, connectivity maintenance [12]–[18] and network integrity maintenance [19]–[21] have been extensively studied, based on simplified channel models. More realistic channel models were considered in [22]–[24], where [22] develops optimal routing algorithms for wireless multihop networks, [23] uses a statistical model to control a group of agents in unexploited areas, and [24] minimizes the end-to-end bit error rate (BER) on a given communication path by relocating relay agents. In addition, several control laws have been developed to move agents to points of interest for, e.g., optimal coverage [25], optimal sensor placement with respect to Fisher information [26], and to maximize sensory information [8], [27]–[29]. In [30], optimal sensor placement using Gaussian processes (GPs) has been addressed.

From [23] and [24], it is clear that proper statistical modeling of the wireless channel is important for connectivity maintenance in both infrastructure-based MAS and cooperative MAS. Moreover, since MAS rely on sensors (e.g., the Global Positioning System (GPS) or ultra-wide band signals) to determine their location, localization errors impact the true channel quality experienced by the MAS. The incorporation of the MAS' location uncertainty in channel modeling and prediction allows to give qualified statements not only on the predicted channel, but also on its expected accuracy in view of the MAS' location accuracy. The wireless channel is usually modeled as being composed by a deterministic part due to path-loss and a stochastic part due to large- and small-scale fading or simply to compensate any model mismatches. Since fading is spatially correlated (e.g., due to obstacles along the propagation path) it is beneficial to exploit the present spatial correlation not only in infrastructure-based MAS, but also in an ad-hoc scenario where cooperative MAS operate. For infrastructure-based MAS, [31], [32] investigated spatial correlation of large-scale fading for outdoor scenarios, and in [31], [33], [34] for indoor scenarios. Many shadowing correlation models have been proposed (see [35] for an overview), among which the Gudmundson model, introduced in [36], is

widely used. For cooperative MAS, [37] proposed an extension of [36] for non-common endpoints, which was supported by channel measurements. This was adapted by [33] in order to address the non-isotropic spatial correlation present in indoor scenarios. A different approach was taken by [38]–[40] where, instead of modeling the shadow variation over space, the loss due to shadowing was considered. When it comes to channel gain prediction for infrastructure-based MAS with respect to (w.r.t.) the present spatial correlation, [23] and [41] among others proposed the usage of GPs. The kriged Kalman filter allows to track spatio-temporal fields [42], [43], where [44] makes use of this filter to track the evolution of the channel gain map. In [45], a Kalman filter was developed to track the temporal evolution of a GP. Note that, for all of these filter-based methods the measurements of the spatio-temporal field are assumed to be recorded at known locations and known time.

The effect of location uncertainty on the prediction quality was studied in [46] and [47]. In [48], a GP-based framework considering location uncertainty of the receiver for robust estimation of the model parameters as well as for channel gain prediction was proposed. In order to incorporate location uncertainty in the GP framework, a similar approach as in [49], [50] was taken. In [51], the framework of [48] was adapted to incorporate location uncertainty of both communication endpoints, though it did not consider the presence of a mean function.

In this paper, we build on [48], [51] and [24], to develop a GP-based approach for learning and prediction of the wireless channel in the presence of location uncertainty, in order to optimize end-to-end communication performance. Our main contributions are:

- A new model for the spatial correlation of transmitter (TX) and receiver (RX) endpoints in large-scale fading through a GP-based framework comprising novel closed-form mean and kernel functions, accounting for uncertain TX and RX locations;
- A novel learning procedure of the underlying channel parameters from measurements collected at arbitrary uncertain TX and RX locations; and
- The incorporation of the above models and procedures in a class of connectivity maintenance problems for cooperative MAS.

Our approach is supported by indoor ad-hoc channel measurements using off-the-shelf technology and extensive numerical simulations.

The remainder of this paper is organized as follows. Section II introduces the model and Section III the problem formulation. Section IV describes the channel and location model, while Section V details our approach for predicting the wireless channel in the presence of such uncertainties. Section VI highlights the applications of channel gain prediction. Simulation results are given in Section VII and conclusions are drawn in Section VIII.

II. SYSTEM MODEL

We consider a MAS of L mobile agents in a workspace $\mathcal{W} \subset \mathbb{R}^2$. The position of agent i is denoted by $\mathbf{q}_i$. The
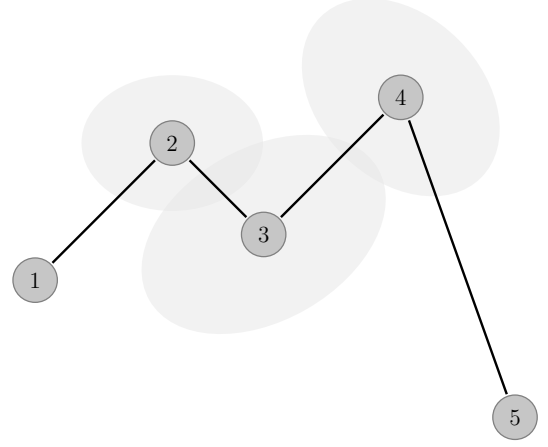

Fig. 1. Communication topology of a cooperative MAS. The communication quality along the route from agent 1 to agent 5 needs to be increased by repositioning controllable agents. Each agent has some location uncertainty due to its imperfect sensor measurements.

agents form a network with associated communication graph $G = (V, E)$ with vertex set $V = \{1, \ldots, L\}$ and edge set $E \subseteq V \times V$. The pairs of positions associated with edge $e \in E$ is denoted by $\mathbf{x}_e = [\mathbf{q}_i^{\mathrm{T}}, \mathbf{q}_{i'}^{\mathrm{T}}]^{\mathrm{T}} \in \mathcal{W}^2$, where (i, i') corresponds to edge e. We will denote by $\mathcal{X}$ the set of all valid configurations of the L mobile agents. To simplify the exposition, we consider V and E to be fixed, i.e., the structure of the communication graph G does not change. A scenario is illustrated in Fig. 1. The communication performance of the network is determined by the quality of a single link and the end-to-end quality, described below.

A. Link Quality

The signal-to-noise ratio (SNR) of a certain link e depends on the transmitting agent, denoted by TX, the receiving agent, denoted by RX, and the wireless propagation channel. It is defined as

$$\gamma(\mathbf{x}_e) = \frac{P_{\mathrm{RX}}^{\mathrm{lin}}(\mathbf{q}_i, \mathbf{q}_{i'})}{N_0 W}, \tag{1}$$

where $P_{\mathrm{RX}}^{\mathrm{lin}}(\mathbf{q}_i, \mathbf{q}_{i'})$ is the received power between the TX located at $\mathbf{q}_i$ and the RX located at $\mathbf{q}_{i'}$ (to be defined in Sec. IV), N_0 denotes the noise power spectral density, and W is the bandwidth of the RX.

B. Network Quality

The end-to-end communication quality depends on the location pairs $\mathbf{X} = [\mathbf{x}_1, \mathbf{x}_2, \ldots, \mathbf{x}_M]$ of all edges $e \in E$, where M is the cardinality of the set E, i.e., $M = |E|$. This can be expressed as

$$J(\mathbf{X}) = \sum_{e \in E} f(\gamma(\mathbf{x}_e)), \tag{2}$$

where $f(\cdot)$ can take on a number of forms, including the following:

- $f(\cdot)$ depends linearly on the SNR, i.e., $f(\gamma(\mathbf{x}_e)) = a_e \gamma(\mathbf{x}_e)$, for constants a_e. Application scenarios include

the maximization of the transmission range for a fixed TX power.

- $f(\cdot)$ depends on the logarithm of the SNR, i.e., $f(\gamma(\mathbf{x}_e)) = a_e \log_2(1 + b_e\gamma(\mathbf{x}_e))$, for constants a_e, b_e, which corresponds to the instantaneous capacity of an AWGN channel in nats/s/Hz [52], [53]. An application scenario includes the maximization of data throughput.
- $f(\cdot)$ depends exponentially on the SNR, i.e., $f(\gamma(\mathbf{x}_e)) = a_e + b_e \exp(-c_e\gamma(\mathbf{x}_e))$, for constants a_e, b_e, c_e. An application scenario includes the maximization of probability of correct reception of a transmitted bit [54, Ch. 9], which is useful for, e.g., minimizing the transmission latency.

We assume that the SNR has been measured at N specific location pairs $\mathbf{X}_N = [\mathbf{x}_1, \mathbf{x}_2, \ldots, \mathbf{x}_N]$. These measurements are available to solve the optimization problem formulated next.

III. PROBLEM FORMULATION

In order to optimize the end-to-end communication quality when the SNR is available for all $\mathbf{X}$ and $\mathbf{X}$ is known precisely, we can consider the following standard optimization problem:

$$\underset{\mathbf{X} \in \mathcal{X}}{\text{maximize}} \; J(\mathbf{X}). \tag{3}$$

In other words, we would like to place the agents in a way such that $J(\mathbf{X})$ is maximized. In practical scenarios, this problem is challenging because of two sources of uncertainty:

- *SNR uncertainty:* The SNR $\gamma(\mathbf{x}_e)$ is generally not known exactly for all $\mathbf{x}_e \in \mathcal{W}^2$. Instead, SNR measurements at a finite set of location pairs $\mathbf{X}_N$ are available, based on which $\gamma(\mathbf{x}_e)$ must be predicted for any $\mathbf{x}_e \in \mathcal{W}^2$.
- *Location uncertainty:* The location of an agent pair may not be known exactly, either for the above-mentioned measurements or when solving (3). We will denote by $\mathbf{u}_e$ the description of the location uncertainty[1] of the location pair $\mathbf{x}_e$, and correspondingly $\mathbf{U}$ for $\mathbf{X}$, and $\mathcal{U}$ for $\mathcal{X}$.

To deal with these different types of uncertainty, instead of (3), we will consider the following optimization problem

$$\underset{\mathbf{U} \in \mathcal{U}}{\text{maximize}} \; \mathbb{E}_{\mathbf{X}|\mathbf{U}} \left\{ \mathbb{E}_{\gamma|\mathbf{X}} \left\{ J(\mathbf{X}) \right\} \right\} \tag{4}$$

$$= \underset{\mathbf{U} \in \mathcal{U}}{\text{maximize}} \sum_{e \in E} \mathbb{E}_{\mathbf{x}_e|\mathbf{u}_e} \left\{ \mathbb{E}_{\gamma|\mathbf{x}_e} \left\{ f(\gamma(\mathbf{x}_e)) \right\} \right\} \tag{5}$$

$$\approx \underset{\mathbf{U} \in \mathcal{U}}{\text{maximize}} \sum_{e \in E} \mathbb{E}_{\gamma|\mathbf{u}_e} \left\{ f(\gamma(\mathbf{u}_e)) \right\}, \tag{6}$$

where the transition from (5) to (6) avoids the expectation w.r.t. the link endpoints location by directly considering the SNR random variable $\gamma(\mathbf{u}_e)$, as a function of the location distribution $\mathbf{u}_e$.

The goal of this paper is to provide an approach to solve problems of the form (6), based on a database of N SNR measurements in the workspace, taken at uncertain locations. Our approach will involve the following steps:

1) Based on the measurements with location uncertainty, the channel model is determined.

---

[1] For instance, $\mathbf{u}_e$ could be a mean and covariance matrix associated with a Gaussian distribution over $\mathbf{x}_e$.

Parameter	Value
No. of RX positions	$10,900$
No. of TX positions	11
ΔRX spacing	0.02 m
ΔTX spacing	1 m
min. TX-RX distance	1 m
P_{TX}	20 dBm
Antenna height	0.85 m
TX frequency	2.422 GHz
Bandwidth	20 MHz

2) Based on the model and the measurements, for any set of location distributions for all nodes, $\mathbf{U} \in \mathcal{U}$, we determine predictions of the associated SNRs for each link $\gamma(\mathbf{u}_e)$ and evaluate the objective.
3) Based on the predicted SNRs, the objective is optimized.

Remark 1. We note that, even though $\mathcal{U}$ and $\mathcal{X}$ are convex sets, and $f(\gamma)$ is monotonic in the SNR γ, (4) is inherently a non-convex optimization problem, due to the arbitrary relationship between γ and $\mathbf{x}_e$, as well as γ and $\mathbf{u}_e$. For that reason, our focus will be on steps 1–2 above.

Remark 2. For the case the structure of the communication graph G is not fixed, e.g., one wants to determine the optimal edge set E jointly with the optimal positions $\mathbf{X}$ using (2), then E will become an optimization variable in (3).

IV. STATISTICAL CHANNEL AND LOCATION MODEL

In this section, we will motivate the use of statistical models for both the wireless channel and the agents' locations.

A. Channel Model

1) Motivation: We have collected ad-hoc indoor channel measurements in a corridor at the Department of Electrical Engineering at Chalmers University of Technology. The TX was placed at different positions along the corridor. On a corridor perpendicular to it, the RX was placed on different positions along a line starting at TX position 6.5 m. For every TX–RX location pair, the received power in dBm was measured using commodity hardware radios of type Netgear N150 Wireless adapter. A total of 10,900 measurements were recorded, with additional measurement parameters stated in Table I. To remove small-scale fading effects (detailed later), the measurements were spatially averaged over a window of 0.4 meters. In Fig. 2, the received power in dBm is shown for different TX–RX locations. We observe high received power for any RX position when the TX position is around 6.5 m. Similarly, for RX positions close to the TX line, a high received power can be observed. This is due to line-of-sight (LOS) between TX and RX for both of these cases. For other TX–RX locations (partly) non-line-of-sight (NLOS) situations occur, where large-scale fading heavily affects the received signal power. From Fig. 2, it is clear that the channel depends in a complex way on the TX and RX location, as well as the propagation environment. It is thus not appropriate to consider $\gamma(\mathbf{x}_e)$ as a simple function of the distance between TX and
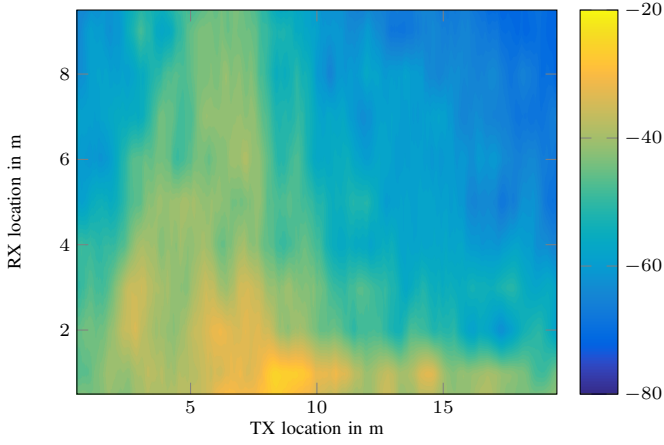
Fig. 2. Measured received signal power in dBm for different TX and RX positions in a mixed LOS/NLOS scenario. The RX moved perpendicular to the TX starting at TX position 6.5 m. Measurements have been spatially averaged to remove small-scale fading.

RX. Instead, we consider $\gamma(\mathbf{x}_e)$ as a realization of a random process, with properly defined statistical properties.

2) Statistical Channel Model: We consider a TX located at $\mathbf{q}_{\mathrm{TX}} \in \mathcal{W}$ which emits a signal with power $P_{\mathrm{TX}}^{\mathrm{lin}}$ (in linear scale), which is transmitted through the wireless channel and is received at the RX located at $\mathbf{q}_{\mathrm{RX}} \in \mathcal{W}$. The transmitted signal experiences distance-dependent path-loss, large-scale fading due to obstacles in the propagation path, and small-scale fading due to multi-path. Following [55, Ch. 2], the received signal power is expressed as

$$P_{\mathrm{RX}}^{\mathrm{lin}}(\mathbf{q}_{\mathrm{TX}}, \mathbf{q}_{\mathrm{RX}}) = P_{\mathrm{TX}}^{\mathrm{lin}} g_0 \, ||\mathbf{q}_{\mathrm{TX}} - \mathbf{q}_{\mathrm{RX}}||_2^{-\eta} \qquad (7)$$
$$\times \, \psi(\mathbf{q}_{\mathrm{TX}}, \mathbf{q}_{\mathrm{RX}}) \, |h(\mathbf{q}_{\mathrm{TX}}, \mathbf{q}_{\mathrm{RX}})|^2,$$

where constant g_0 captures antenna and other propagation gains, η denotes the path-loss exponent, $\psi(\mathbf{q}_{\mathrm{TX}}, \mathbf{q}_{\mathrm{RX}})$ is the TX and RX position dependent shadowing and $h(\mathbf{q}_{\mathrm{TX}}, \mathbf{q}_{\mathrm{RX}})$ captures small-scale fading effects. Under the assumption that measurements average out small-scale fading, either in time (measurements taken over a time window), frequency (measurements represent average power over a large frequency band), or space (by using multiple antennas) the received signal power in dBm is reduced to

$$P_{\mathrm{RX}}(\mathbf{q}_{\mathrm{TX}}, \mathbf{q}_{\mathrm{RX}}) = L_0 - 10\eta \log_{10} ||\mathbf{q}_{\mathrm{TX}} - \mathbf{q}_{\mathrm{RX}}||_2 \quad (8)$$
$$+ \Psi(\mathbf{q}_{\mathrm{TX}}, \mathbf{q}_{\mathrm{RX}}),$$

where $L_0 = P_{\mathrm{TX}} + 10\log_{10}(g_0) + 10\eta \log_{10}(d_0)$, and $\Psi(\mathbf{q}_{\mathrm{TX}}, \mathbf{q}_{\mathrm{RX}}) = 10\log_{10} \psi(\mathbf{q}_{\mathrm{TX}}, \mathbf{q}_{\mathrm{RX}})$. We assume that the large-scale fading (shadowing) follows a log-normal distribution, i.e., $\Psi(\mathbf{q}_{\mathrm{TX}}, \mathbf{q}_{\mathrm{RX}}) \sim \mathcal{N}(0, \sigma_\Psi^2)$, where σ_Ψ^2 is the shadowing variance [54]. For a static environment and homogeneous TX and RX units, the transmission channel can be considered reciprocal and hence, $\Psi(\mathbf{q}_{\mathrm{TX}}, \mathbf{q}_{\mathrm{RX}}) = \Psi(\mathbf{q}_{\mathrm{RX}}, \mathbf{q}_{\mathrm{TX}})$ (c.f. [54], [55]).

Remark 3. In general, shadowing is spatially correlated, i.e., RX locations which are spatially close experience similar shadow fading [35], [36]. For a common TX endpoint $\mathbf{q}_{\mathrm{TX}} \in \mathcal{W}$, a well-known correlation model is the Gudmundson model

for different RX locations $\mathbf{q}_{\mathrm{RX},i}, \mathbf{q}_{\mathrm{RX},j} \in \mathcal{W}$ [36]. This model can be extended to account for ad-hoc communication links with non-common TX endpoints $\mathbf{q}_{\mathrm{TX},k}, \mathbf{q}_{\mathrm{TX},l} \in \mathcal{W}$ (see, for example [33], [37]), under the assumption that the TX–RX transmitter distance is large compared to the displacement between TX endpoints and the RX endpoints.

Remark 4. The presence of multiple agents operating in the workspace $\mathcal{W}$ will cause small scale propagation effects, but do not affect the (average) received power P_{RX}. For this reason, we consider in this work the environment to be static during the operation of the MAS. A possible extension of this work could for instance address also the temporal evolution of the shadowing field with the help of a kriged Kalman filter [42], [43] for the case the shadowing field cannot be assumed to be static such as, e.g., in a factory building where large moving objects are present. In doing so, the available measurements recorded at location pairs $\mathbf{X}_N$ need not be outdated. This can be achieved when agents periodically measure the received signal power w.r.t. their neighbors and only up to date measurements are used to solve (6).

B. Location Model

1) Motivation: Agents rely on sensors to determine their location with the effect that their estimated position has some residual uncertainty. For our problem, this has two implications. First, when measuring the SNR at a specific location pair $\mathbf{x} = [\mathbf{q}_{\mathrm{TX}}^{\mathrm{T}}, \mathbf{q}_{\mathrm{RX}}^{\mathrm{T}}]^{\mathrm{T}}$, the true measurement locations are not known. Secondly, in the workspace, the quality of the positioning system may vary. As an example, when using GPS, the number of available satellites and their geometry will be location-dependent. Consequently, there may be parts of the workspace where location accuracy is low, thus deteriorating the accuracy of SNR predictions.

2) Statistical Location Model: We will model the location uncertainty through Gaussian distributions, as this is compatible with most localization/navigation approaches, including the Kalman filter and extended Kalman filter [56]. Hence, the statistical model for the uncertainty of a link location pair $\mathbf{x}$ is given by

$$\mathbf{x} \sim \mathcal{N}(\boldsymbol{\mu}, \boldsymbol{\Sigma}), \qquad (9)$$

in which $\boldsymbol{\mu} = [\boldsymbol{\mu}_{\mathrm{TX}}^{\mathrm{T}}, \boldsymbol{\mu}_{\mathrm{RX}}^{\mathrm{T}}]^{\mathrm{T}} \in \mathbb{R}^4$ and $\boldsymbol{\Sigma} = \mathrm{diag}\,(\boldsymbol{\Sigma}_{\mathrm{TX}}, \boldsymbol{\Sigma}_{\mathrm{RX}})$. Note that the TX and RX location are considered as independent random variables.

V. CHANNEL GAIN PREDICTION

In this section, we describe how to predict the SNR for a target TX and RX location pair $\mathbf{x}_e$ using GPs, based on a measurement database. We first consider the case without location uncertainty (Section V-A, where we detail conventional GP – cGP) and then with location uncertainty (Section V-B, where we detail uncertain GP – uGP). We assume the reader has a working knowledge of GPs. For an introduction on GPs the reader is referred to [57], [58, Ch. 6.4].
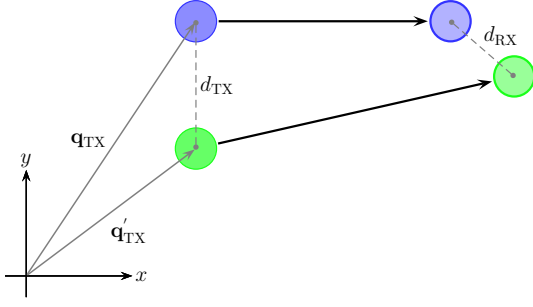
Fig. 3. Illustration of TX and RX displacement between two TX-RX pairs $\mathbf{x}$ and $\mathbf{x}'$ in $\mathbb{R}^2$. The TX displacement is $d_{\text{TX}} = \|\mathbf{q}_{\text{TX}} - \mathbf{q}'_{\text{TX}}\|_2$ and the RX displacement is $d_{\text{RX}} = \|\mathbf{q}_{\text{RX}} - \mathbf{q}'_{\text{RX}}\|_2$.

A. Perfect Location Information (cGP)

1) Model: Let $\mathbf{x}, \mathbf{x}' \in \mathcal{W}^2$ and denote the corresponding received power by $P_{\text{RX}}(\mathbf{x}) \triangleq P_{\text{RX}}(\mathbf{q}_{\text{TX}}, \mathbf{q}_{\text{RX}})$. We model the received signal power as the GP

$$P_{\text{RX}}(\mathbf{x}) \sim \mathcal{GP}(\mu_{\text{cGP}}(\mathbf{x}), c_{\text{cGP}}(\mathbf{x}, \mathbf{x}')), \quad (10)$$

where $\mu_{\text{cGP}}(\mathbf{x}) : \mathcal{W}^2 \to \mathbb{R}$ denotes the mean function and $c_{\text{cGP}}(\mathbf{x}, \mathbf{x}') : \mathcal{W}^2 \times \mathcal{W}^2 \to \mathbb{R}^+$ the covariance function (also referred to as kernel). The mean $\mu_{\text{cGP}}(\mathbf{x})$ is obtained by computing the expectation of (8) w.r.t. the large-scale fading $\Psi(\mathbf{x})$, yielding

$$\mu_{\text{cGP}}(\mathbf{x}) = L_0 - 10\eta \log_{10} \|\mathbf{q}_{\text{TX}} - \mathbf{q}_{\text{RX}}\|_2. \quad (11)$$

The covariance function $c_{\text{cGP}}(\mathbf{x}, \mathbf{x}')$ describes the spatial correlation of large-scale fading between any two pairs of communication links $\mathbf{x}, \mathbf{x}' \in \mathcal{W}^2$. In Fig. 3, two communication links together with their TX and RX displacement are illustrated. Following [33], [37], assuming the channel is isotropic, the spatial channel correlation can be explained by the Euclidean distance of the link endpoints, i.e., for two links with locations $\mathbf{x}$ and $\mathbf{x}'$, the correlation is characterized by the distance between the two TXs $d_{\text{TX}} = \|\mathbf{q}_{\text{TX}} - \mathbf{q}'_{\text{TX}}\|_2$ and between the two RXs $d_{\text{RX}} = \|\mathbf{q}_{\text{RX}} - \mathbf{q}'_{\text{RX}}\|_2$. Further, we assume that d_{TX} and d_{RX} are small compared to distances between TXs and RXs such that only those have a significant spatial correlation. Otherwise, the resulting covariance matrix (to be defined) may not be Positive Semi-Definite (PSD) anymore [38]. Finally, in many ad-hoc networks, agents have an identical configuration in terms of communication hardware, and hence channel reciprocity holds (i.e., $P_{\text{RX}}(\mathbf{q}_{\text{TX}}, \mathbf{q}_{\text{RX}}) = P_{\text{RX}}(\mathbf{q}_{\text{RX}}, \mathbf{q}_{\text{TX}})$), implying that the covariance function should be invariant to exchanges of TX and RX per link. Based on these requirement, we propose to extend the kernel of [48] by a kernel considering the correlation of the TX locations as well:

$$c_{\text{cGP}}(\mathbf{x}, \mathbf{x}') = \begin{cases} \sigma_{\text{proc}}^2 + \sigma_{\Psi}^2, & \mathbf{x} = \mathbf{x}', \\ \sigma_{\Psi}^2 \exp\left(-\frac{d_{\text{TX}}^{\kappa} + d_{\text{RX}}^{\kappa}}{d_c^{\kappa}}\right), & \text{else,} \end{cases} \quad (12)$$

under the assumption that

$$d_{\text{TX}}, d_{\text{RX}} \ll \quad (13)$$
$$\min\{\|\mathbf{q}_{\text{TX}} - \mathbf{q}_{\text{RX}}\|, \|\mathbf{q}_{\text{TX}} - \mathbf{q}'_{\text{RX}}\|, \|\mathbf{q}'_{\text{TX}} - \mathbf{q}_{\text{RX}}\|, \|\mathbf{q}'_{\text{TX}} - \mathbf{q}'_{\text{RX}}\|\}.$$

Note, from (12) the kernel of [48] is obtained when $d_{\text{TX}} = 0$, i.e., $\mathbf{q}_{\text{TX}} = \mathbf{q}'_{\text{TX}}$. In (12), d_c is referred to as the kernel width or decorrelation distance, σ_{Ψ}^2 is the shadowing variance, and σ_{proc}^2 models any residual perturbations. Setting the parameter $\kappa = 1$, (12) yields the model of [37], while for $\mathbf{q}_{\text{TX}} = \mathbf{q}'_{\text{TX}}$, the commonly used model of [36] is obtained. Following [48] and setting $\kappa = 2$, we obtain the squared exponential kernel, which will be useful in the subsequent sections. For $\mathbf{x} = \mathbf{x}'$, the first part of (12) models any white noise not due to measurement noise (e.g., caused by kernel mismatch) with power σ_{proc}^2. The full hyper-parameter vector of the cGP-method is

$$\boldsymbol{\theta} = [L_0, \eta, \sigma_{\text{proc}}, d_c, \sigma_{\Psi}]^{\text{T}}, \quad (14)$$

assuming the receiver noise power σ_n^2 is known and κ is given.

2) Prediction: Let us assume we have a training database $\mathcal{D}$ comprising N measurements $y_i = P_{\text{RX}}(\mathbf{x}_i) + n_i$, recorded for links $\mathbf{x}_i$, $i = 1, \ldots, N$ with $n_i \sim \mathcal{N}(0, \sigma_n^2)$. We wish to predict the received power for a test link $\mathbf{x}_*$. The mean and variance of the received power along the test link can be expressed in closed form as [57]

$$\mathbb{E}\{P_{\text{RX}}(\mathbf{x}_*)|\mathcal{D}, \boldsymbol{\theta}, \mathbf{x}_*\} = \mu_{\text{cGP}}(\mathbf{x}_*) + \mathbf{k}_*^{\text{T}} \mathbf{K}^{-1}(\mathbf{y} - \boldsymbol{\mu}), \quad (15)$$
$$\mathbb{V}\{P_{\text{RX}}(\mathbf{x}_*)|\mathcal{D}, \boldsymbol{\theta}, \mathbf{x}_*\} = \sigma_{\text{proc}}^2 + \sigma_{\Psi}^2 - \mathbf{k}_*^{\text{T}} \mathbf{K}^{-1} \mathbf{k}_*, \quad (16)$$

in which

$$\mathbf{y} = [y_1, y_2, \ldots, y_N]^{\text{T}},$$
$$\boldsymbol{\mu} = [\mu_{\text{cGP}}(\mathbf{x}_1), \ldots, \mu_{\text{cGP}}(\mathbf{x}_N)]^{\text{T}},$$
$$\mathbf{k}_* = [c_{\text{cGP}}(\mathbf{x}_1, \mathbf{x}_*), c_{\text{cGP}}(\mathbf{x}_2, \mathbf{x}_*), \ldots, c_{\text{cGP}}(\mathbf{x}_N, \mathbf{x}_*)]^{\text{T}},$$

and PSD $\mathbf{K} \in \mathbb{R}^{N \times N}$, with

$$\mathbf{K}_{ij} = c_{\text{cGP}}(\mathbf{x}_i, \mathbf{x}_j) + \sigma_n^2 \delta_{i,j}, \quad (17)$$

where $\delta_{i,j} = 1$ when $i = j$ and $\delta_{i,j} = 0$ otherwise.

Remark 5. The channel gain prediction, as introduced above, does not assume channel reciprocity per se. With the definition of the input vector $\mathbf{x} = [\mathbf{q}_{\text{TX}}, \mathbf{q}_{\text{RX}}]^{\text{T}}$, we introduced an implicit ordering, where channel reciprocity in the prediction step of cGP is not considered. The introduction of this property into the cGP model can be done: (i) by applying an operator on $\mathbf{x}$ [57], [58] to make it independent of the TX–RX link direction, (ii) by modifying the kernel function as it has been proposed in [23], or (iii) by extending the training database $\mathcal{D}$ by its reciprocal counterpart, where for each measurement y_i the role of TX and RX in state $\mathbf{x}_i$ is interchanged. Note that, for methods (i) and (ii) the resulting covariance matrix incorporating all N measurements needs to be PSD. This may not be ensured in (ii). In this work, we implement method (iii) over (i) due to its simplicity and because it increases the size of the training database by a factor of two.

3) Learning model parameters: The cGP prediction above assumes $\boldsymbol{\theta}$ is known. In practice, $\boldsymbol{\theta}$ is either set by an expert or needs to be estimated from the database $\mathcal{D}$. The joint probability density function (pdf) of observations $\mathbf{y}$ and location pairs $\mathbf{X}_N$ has a Gaussian form with mean $\boldsymbol{\mu}$ and covariance matrix $\mathbf{K}$. Since both $\boldsymbol{\mu}$ and $\mathbf{K}$ depend on $\boldsymbol{\theta}$, we write $\boldsymbol{\mu}_{\boldsymbol{\theta}}$ and $\mathbf{K}_{\boldsymbol{\theta}}$, i.e.,

$$\mathbf{y}|\mathbf{X}_N, \boldsymbol{\theta} \sim \mathcal{N}(\boldsymbol{\mu}_{\boldsymbol{\theta}}, \mathbf{K}_{\boldsymbol{\theta}}). \quad (18)$$

Now, $\boldsymbol{\theta}$ can be estimated by maximizing the log-likelihood w.r.t. $\boldsymbol{\theta}$. To find a closed-form expression for $\boldsymbol{\theta}$ can be challenging [41].

Remark 6. In [41], [48] a sub-optimal but simpler approach to estimate the channel parameters $\boldsymbol{\theta}$ has been proposed. First, the deterministic path-loss parameters $\boldsymbol{\alpha} = [L_0, \eta]^\mathrm{T}$ are estimated and subsequently the kernel parameters $\boldsymbol{\beta} = [\sigma_{\mathrm{proc}}, d_c, \sigma_\Psi]^\mathrm{T}$, based on the estimate of $\boldsymbol{\alpha}$. The least squares (LS) estimate of $\boldsymbol{\alpha}$ with cost function $S(\boldsymbol{\alpha}) = ||\mathbf{y} - \mathbf{F}\boldsymbol{\alpha}||_2^2$ has the solution

$$\hat{\boldsymbol{\alpha}} = (\mathbf{F}^\mathrm{T}\mathbf{F})^{-1}\mathbf{F}^\mathrm{T}\mathbf{y}, \tag{19}$$

where $\mathbf{F} = [\mathbf{1}_N, -\mathbf{d}]$ and $\mathbf{d} = 10[\log_{10}||\mathbf{q}_{\mathrm{TX},1} - \mathbf{q}_{\mathrm{RX},1}||_2, \ldots, \log_{10}||\mathbf{q}_{\mathrm{TX},N} - \mathbf{q}_{\mathrm{RX},N}||_2]^\mathrm{T}$. With the estimation of $\boldsymbol{\alpha}$, a maximum likelihood estimation of $\boldsymbol{\beta}$ on the zero-mean measurements can be carried out. The zero-mean measurements are obtained by

$$\mathbf{y}_c = \mathbf{y} - \mathbf{F}\hat{\boldsymbol{\alpha}}. \tag{20}$$

Since $\mathbf{y}_c$ is now a zero-mean Gaussian random variable with covariance matrix $\mathbf{K}_{\boldsymbol{\theta}}$, we obtain an estimate of $\boldsymbol{\beta}$ by minimizing the negative log-likelihood according to

$$\hat{\boldsymbol{\beta}} = \arg\min_{\boldsymbol{\beta}} (\log|\mathbf{K}_{\boldsymbol{\theta}}| + \mathbf{y}_c^\mathrm{T}\mathbf{K}_{\boldsymbol{\theta}}^{-1}\mathbf{y}_c). \tag{21}$$

Following [48], we first obtain the variance in $\mathbf{y}_c$ by $\sigma_{\mathrm{tot}}^2 = \frac{1}{N}\mathbf{y}_c^\mathrm{T}\mathbf{y}_c$, where $\sigma_{\mathrm{tot}}^2 = \sigma_{\mathrm{proc}}^2 + \sigma_n^2 + \sigma_\Psi^2$ holds. Since in general the likelihood may be non-convex, we then find $\hat{\boldsymbol{\beta}}$ through a global search over the domain of σ_Ψ and d_c (σ_{proc} is uniquely defined through σ_{tot}).

Following this approach, we have estimated the channel parameters for the ad-hoc channel measurements from Section IV with $\kappa = 1$: from the raw measurement data, we found $\hat{L}_0 = -20.42$ dBm, $\hat{\eta} = 3.59$, $\hat{d}_c = 3.61$ m, $\hat{\sigma}_{\mathrm{proc}} = 3.74$, and $\hat{\sigma}_\Psi = 6.46$. After spatial averaging over a 0.4 m window, these values became $\hat{L}_0 = -20.21$ dBm, $\hat{\eta} = 3.61$, $\hat{d}_c = 3.93$ m, $\hat{\sigma}_{\mathrm{proc}} = 0$, and $\hat{\sigma}_\Psi = 6.35$. Note, for this estimation we used a random subset of only 6% of the measurement data, which was found to be sufficient to produce robust estimates.

B. Uncertain Location Information (uGP)

So far we introduced cGP to predict the channel for arbitrary (perfectly known) TX and RX locations. We now extend cGP, to incorporate uncertain location information and call it uGP. In doing so, we make use of the *location distribution* of the TX and RX. This allows us to obtain a GP model which incorporates location uncertainty into the channel prediction and provides closed-form expressions for the mean and variance of the prediction. Note that uGP was introduced in [48] for a common TX endpoint, and extended in [51] to non-common TX endpoints yet no closed-form expression for the GP mean function was provided. Here, we provide a general and unified closed-form channel prediction framework to incorporate location uncertainty of training and test data.

1) Model: Assume the pdf of the TX and RX location is Gaussian, i.e., $p(\mathbf{q}_{\mathrm{TX}}) = \mathcal{N}(\boldsymbol{\mu}_{\mathrm{TX}}, \boldsymbol{\Sigma}_{\mathrm{TX}})$ and $p(\mathbf{q}_{\mathrm{RX}}) = \mathcal{N}(\boldsymbol{\mu}_{\mathrm{RX}}, \boldsymbol{\Sigma}_{RX})$. Additionally, $\boldsymbol{\Sigma}_{\mathrm{TX}}$ is assumed to have equal variance σ_{TX}^2 in each dimension, and so does $\boldsymbol{\Sigma}_{\mathrm{RX}}$ with variance σ_{RX}^2. For readability, we collect the distribution parameters in a vector $\mathbf{u} = [\mathbf{u}_{\mathrm{TX}}^\mathrm{T}, \mathbf{u}_{\mathrm{RX}}^\mathrm{T}]^\mathrm{T}$ with $\mathbf{u}_{\mathrm{TX}} = [\boldsymbol{\mu}_{\mathrm{TX}}^\mathrm{T}, \sigma_{\mathrm{TX}}]^\mathrm{T}$, and similarly for $\mathbf{u}_{\mathrm{RX}}$. Further, we model the received power in dBm through a GP over the vector $\mathbf{u}$ by

$$P_{\mathrm{RX}}(\mathbf{u}) \sim \mathcal{GP}(\mu_{\mathrm{uGP}}(\mathbf{u}), c_{\mathrm{uGP}}(\mathbf{u}, \mathbf{u}')), \tag{22}$$

with the mean function $\mu_{\mathrm{uGP}}(\mathbf{u}) : \mathcal{U} \to \mathbb{R}$ and a PSD covariance $c_{\mathrm{uGP}}(\mathbf{u}, \mathbf{u}') : \mathcal{U} \times \mathcal{U} \to \mathbb{R}^+$. Building on the cGP mean function, the uGP mean function becomes

$$\mu_{\mathrm{uGP}}(\mathbf{u}) = \mathbb{E}_{\mathbf{x}|\mathbf{u},\Psi(\mathbf{x})}\{P_{\mathrm{RX}}(\mathbf{x})\}, \tag{23}$$

where we now need to take the expectation not only over the large-scale fading $\Psi(\mathbf{x})$, but also on the location $\mathbf{x}$. Since $\mathbb{E}_{\Psi(\mathbf{x})}\{\Psi(\mathbf{x})\} = 0$ (c.f. (8)), we are left with the expectation w.r.t. the location $\mathbf{x}$ in (8).

Theorem 1. The uGP mean function is available in closed-form and is given by

$$\begin{aligned} \mu_{\mathrm{uGP}}(\mathbf{u}) &= L_0 - \frac{5\eta}{\ln 10} \\ &\times \left[\ln(|\mu_*|^2) - E_i(-|\mu_*|^2) + \ln(2\sigma^2)\right], \end{aligned} \tag{24}$$

where $\mu_* = \frac{\mu_1 + j\mu_2}{\sigma\sqrt{2}}$, $[\mu_1, \mu_2]^\mathrm{T} = \boldsymbol{\mu}_{\mathrm{TX}} - \boldsymbol{\mu}_{\mathrm{RX}}$, $\sigma^2 = \sigma_{\mathrm{TX}}^2 + \sigma_{\mathrm{RX}}^2$, and the function $E_i(\cdot)$ denotes the exponential integral function

$$E_i(-x) = -\int_x^\infty \frac{e^{-t}}{t}\mathrm{d}t, \ x > 0. \tag{25}$$

Proof: See Appendix A. ∎

The evaluation of the covariance function is more involved. Starting from cGP, the uGP covariance function becomes

$$\begin{aligned} &c_{\mathrm{uGP}}(\mathbf{u}, \mathbf{u}') \\ &= \begin{cases} \iint c_{\mathrm{cGP}}(\mathbf{x}, \mathbf{x}')p(\mathbf{x})p(\mathbf{x}')\mathrm{d}\mathbf{x}\mathrm{d}\mathbf{x}', & \mathbf{u} \neq \mathbf{u}' \\ \int c_{\mathrm{cGP}}(\mathbf{x}, \mathbf{x})p(\mathbf{x})\mathrm{d}\mathbf{x} + \sigma_{\mathrm{mean}}^2(\mathbf{u}) & \mathbf{u} = \mathbf{u}', \end{cases} \end{aligned} \tag{26}$$

where $p(\mathbf{x})$ denotes the pdf w.r.t. random variable $\mathbf{x}$, $c_{\mathrm{cGP}}(\cdot, \cdot)$ is the covariance function under perfect location information stated in (12), and $\sigma_{\mathrm{mean}}^2(\mathbf{u})$ captures the contribution to the output uncertainty due to the non-zero mean function.[2]

Since one of the advantages of using GPs is the availability of closed form expressions for the prediction, we would like to have a closed form expression for (26). In doing so, we rely on the squared exponential kernel, i.e., where $\kappa = 2$ in (12) and the restriction that the TX and RX locations in $\mathbf{x}$ are independent and Gaussian. Then, (26) can be expressed in closed form [50], [51], [58] as

$$\begin{aligned} &c_{\mathrm{uGP}}(\mathbf{u}, \mathbf{u}') \\ &= \begin{cases} \frac{\sigma_\Psi^2}{\sqrt{|\boldsymbol{\Gamma}_{\mathrm{TX}}||\boldsymbol{\Gamma}_{\mathrm{RX}}|}} e^{-\frac{\boldsymbol{\Delta}_{\mathrm{TX}}^\mathrm{T}\boldsymbol{\Gamma}_{\mathrm{TX}}^{-1}\boldsymbol{\Delta}_{\mathrm{TX}} + \boldsymbol{\Delta}_{\mathrm{RX}}^\mathrm{T}\boldsymbol{\Gamma}_{\mathrm{RX}}^{-1}\boldsymbol{\Delta}_{\mathrm{RX}}}{d_c^2}} & \mathbf{u} \neq \mathbf{u}' \\ \sigma_{\mathrm{proc}}^2 + \sigma_\Psi^2 + \sigma_{\mathrm{mean}}^2(\mathbf{u}) & \mathbf{u} = \mathbf{u}', \end{cases} \end{aligned} \tag{27}$$

[2]For instance, when there is no shadowing (i.e., $\sigma_\Psi = 0$), it is readily seen that $\sigma_{\mathrm{mean}}^2(\mathbf{u})$ corresponds to the uncertainty in the path loss, due to uncertainty in the location.

where $\boldsymbol{\Gamma}_{\text{TX}} = (\mathbf{I} + d_c^{-2}(\boldsymbol{\Sigma}_{\text{TX}} + \boldsymbol{\Sigma}'_{\text{TX}}))$, $\boldsymbol{\Delta}_{\text{TX}} = \boldsymbol{\mu}_{\text{TX}} - \boldsymbol{\mu}'_{\text{TX}}$, and similarly for the RX. Here, $\mathbf{I}$ denotes the identity matrix of suitable size. In contrast to (12), uGP works on the parameters of the distribution of $\mathbf{x}$ instead of the state itself. This means that TX distance d_{TX} and RX distance d_{RX} are now the distances between the means given by $\boldsymbol{\Delta}_{\text{TX}}$ and $\boldsymbol{\Delta}_{\text{RX}}$, respectively (c.f. Fig. 3). The role of $\boldsymbol{\Sigma}_{\text{TX}}$ and $\boldsymbol{\Sigma}_{\text{RX}}$ in (27) is to increase the kernel width as location uncertainty increases. In this way, the decorrelation distance d_c, a channel parameter, remains decoupled from the state (location) uncertainty. The full hyper-parameter vector for uGP is the same as for cGP; see (14).

To determine $\sigma_{\text{mean}}^2(\mathbf{u})$, we must consider the statistics of

$$e_{\text{mean}}(\mathbf{u}) = \mu_{\text{cGP}}(\mathbf{x}) - \mu_{\text{uGP}}(\mathbf{u}), \qquad (28)$$

where $\mathbf{x} \sim \mathcal{N}(\boldsymbol{\mu}, \boldsymbol{\Sigma})$ is considered as a random variable. In general, $e_{\text{mean}}(\mathbf{u})$ is not Gaussian, due to the nonlinear nature of $\mu_{\text{cGP}}(\mathbf{x})$. By linearizing $\mu_{\text{cGP}}(\mathbf{x})$ around the mean of $\mathbf{x}$, we can approximate

$$e_{\text{mean}}(\mathbf{u}) \approx \mu_{\text{cGP}}(\boldsymbol{\mu}) - \mu_{\text{uGP}}(\mathbf{u}) \qquad (29)$$
$$+ \nabla_{\mathbf{x}}^{\text{T}} \mu_{\text{cGP}}(\mathbf{x})|_{\mathbf{x}=\boldsymbol{\mu}}(\mathbf{x} - \boldsymbol{\mu}),$$

so that, due to the Gaussian nature of $\mathbf{x}$,

$$e_{\text{mean}}(\mathbf{u}) \sim \qquad (30)$$
$$\mathcal{N}(\mu_{\text{cGP}}(\boldsymbol{\mu}) - \mu_{\text{uGP}}(\mathbf{u}), \underbrace{|\nabla_{\mathbf{x}}^{\text{T}} \mu_{\text{cGP}}(\mathbf{x})|_{\mathbf{x}=\boldsymbol{\mu}} \boldsymbol{\Sigma}^{1/2}|^2}_{=\sigma_{\text{mean}}^2(\mathbf{u})}),$$

which can easily be computed for any $\mathbf{u}$. Note that when there is no position uncertainty, or when $\mu_{\text{cGP}}(\mathbf{x})$ is constant, we find that $e_{\text{mean}}(\mathbf{u})$ is identically equal to zero, as expected. Observe also that when $\mu_{\text{cGP}}(\mathbf{x})$ is linear in $\mathbf{x}$, the Gaussian model for $e_{\text{mean}}(\mathbf{u})$ in (30) is exact.

Remark 7. When the uncertainty regarding the locations $\sigma_{\text{TX}}^2, \sigma_{\text{RX}}^2 \to 0$, the expressions for mean and covariance in uGP revert back to the corresponding expressions in cGP with $\kappa = 2$.

2) Prediction: In contrast to cGP, we now need the pdfs on the TX and RX position of the recorded measurements. Then, the training database $\mathcal{D}$ comprises N measurements with $\mathbf{U} = [\mathbf{u}_1, \mathbf{u}_2, \ldots, \mathbf{u}_N]$ and $\mathbf{y}$ as defined previously. For a test location pdf $\mathbf{u}_*$, comprising a test TX and RX pdf, the predicted mean and variance of $P_{\text{RX}}(\mathbf{u}_*)$ are given by [50]

$$\mathbb{E}\{P_{\text{RX}}(\mathbf{u}_*)|\mathcal{D}, \boldsymbol{\theta}, \mathbf{u}_*\} = \mu_{\text{uGP}}(\mathbf{u}_*) + \mathbf{k}_*^{\text{T}} \mathbf{K}^{-1}(\mathbf{y} - \boldsymbol{\mu}), (31)$$
$$\mathbb{V}\{P_{\text{RX}}(\mathbf{u}_*)|\mathcal{D}, \boldsymbol{\theta}, \mathbf{u}_*\} = \sigma_{\text{mean}}^2(\mathbf{u}_*) + \sigma_{\text{proc}}^2 + \sigma_{\Psi}^2$$
$$- \mathbf{k}_*^{\text{T}} \mathbf{K}^{-1} \mathbf{k}_*, \qquad (32)$$

where $\mathbf{k}_* = [c_{\text{uGP}}(\mathbf{u}_1, \mathbf{u}_*), c_{\text{uGP}}(\mathbf{u}_2, \mathbf{u}_*), \ldots, c_{\text{uGP}}(\mathbf{u}_N, \mathbf{u}_*)]^{\text{T}}$, $\boldsymbol{\mu} = [\mu_{\text{uGP}}(\mathbf{u}_1), \mu_{\text{uGP}}(\mathbf{u}_2), \ldots, \mu_{\text{uGP}}(\mathbf{u}_N)]^{\text{T}}$ and $\mathbf{K}$ is as in (17), replacing the cGP kernel with the uGP kernel (27).

Remark 8. It is clear that channel prediction for uGP is similar to cGP, except for a different input space (distributions over locations instead of locations themselves) and accordingly, different mean and covariance functions. In particular, the discussion regarding channel reciprocity from cGP still holds.

3) Learning model parameters: Similar to cGP, we would like to decompose the learning procedure to first estimate $\boldsymbol{\alpha} = [L_0, \eta]^{\text{T}}$ and then $\boldsymbol{\beta} = [\sigma_{\text{proc}}, d_c, \sigma_{\Psi}]^{\text{T}}$. We can express each measurement, which is taken at an unknown location, as

$$y_i = \mu_{\text{uGP}}(\mathbf{u}_i) + n_i + w_i(\mathbf{u}_i) + e_{\text{mean}}(\mathbf{u}_i), \qquad (33)$$

where $\mu_{\text{uGP}}(\mathbf{u}_i) = \mathbb{E}_{\mathbf{x}}\{\mathbf{f}(\mathbf{x}_i)\}^{\text{T}} \boldsymbol{\alpha}$ is defined in (24), $\mathbf{f}(\mathbf{x}_i) = [1, -10\log_{10}\|\mathbf{q}_{\text{TX},i} - \mathbf{q}_{\text{RX},i}\|]^{\text{T}}$, n_i is the zero mean measurement noise with variance σ_n^2, $w_i(\mathbf{u}_i)$ is zero mean spatially correlated noise originated from shadowing with covariance function (27), and $e_{\text{mean}}(\mathbf{u}_i)$ was introduced in (29).

Substituting (29) into (33) and introducing $\mathbf{J}(\mathbf{u}_i) = \nabla_{\mathbf{x}_i}^{\text{T}} \mathbf{f}(\mathbf{x}_i)|_{\mathbf{x}_i=\boldsymbol{\mu}_i} \in \mathbb{R}^{2 \times 4}$, we can express the observation as

$$y_i = \mathbf{f}(\boldsymbol{\mu}_i)^{\text{T}} \boldsymbol{\alpha} + z_i, \qquad (34)$$

where z_i is modeled as a zero-mean GP consisting of three components: (i) measurement noise n_i with variance σ_n^2, (ii) white Gaussian mean-induced output noise with variance $\sigma_{\text{mean}}^2(\mathbf{u}_i) = \boldsymbol{\alpha}^{\text{T}} \mathbf{J}(\mathbf{u}_i) \boldsymbol{\Sigma}_i \mathbf{J}^{\text{T}}(\mathbf{u}_i) \boldsymbol{\alpha}$; (iii) spatially correlated noise $w_i(\mathbf{u}_i)$ with covariance function (27) (without $\sigma_{\text{mean}}^2(\mathbf{u}_i)$). To estimate $\boldsymbol{\alpha}$ we can consider the following weighted least squares (WLS) problem

$$\hat{\boldsymbol{\alpha}} = \arg\min_{\boldsymbol{\alpha}} \sum_{i=1}^{N} \frac{(y_i - \mathbf{f}(\boldsymbol{\mu}_i)^{\text{T}} \boldsymbol{\alpha})^2}{\sigma_n^2 + \sigma_{\text{mean}}^2(\mathbf{u}_i) + \sigma_{\Psi}^2 + \sigma_{\text{proc}}^2}. \qquad (35)$$

Note that the denominators in (35) depend on σ_{Ψ} and σ_{proc}, which are unknown, and on $\sigma_{\text{mean}}^2(\mathbf{u}_i)$, which in turn depends on $\boldsymbol{\alpha}$. To get around these dependencies, we propose the following procedure:

1) Given: initial estimate of σ_{Ψ}, σ_{proc} and $\boldsymbol{\alpha}$
2) Substitute the estimates of σ_{Ψ}, σ_{proc}, $\boldsymbol{\alpha}$ in the denominators of (35). Solve (35) for $\boldsymbol{\alpha}$ using standard closed-form WLS.
3) Remove the mean from the observations to obtain $z_i = y_i - \mathbf{f}(\boldsymbol{\mu}_i)^{\text{T}} \boldsymbol{\alpha}$. Now $\mathbf{z} = [z_1, \ldots, z_N]^{\text{T}}$ has a Gaussian distribution with mean zero and covariance matrix $\mathbf{K}_{\boldsymbol{\beta}}$, obtained from (27). Perform a maximum likelihood (ML) estimate for $\boldsymbol{\beta} = [\sigma_{\text{proc}}, d_c, \sigma_{\Psi}]^{\text{T}}$:

$$\hat{\boldsymbol{\beta}} = \arg\min_{\boldsymbol{\beta}} \left(\log|\mathbf{K}_{\boldsymbol{\beta}}| + \mathbf{z}^{\text{T}} \mathbf{K}_{\boldsymbol{\beta}} \mathbf{z}\right). \qquad (36)$$

4) Go back to step 2 until a predetermined number of iterations is exceeded.

Step 2 can be executed multiple times to obtain a better estimate of $\boldsymbol{\alpha}$ and step 4 can be omitted if the procedure is to occur once.

Remark 9. uGP can also be used for cases where (i) position knowledge is perfect in the training database, but not during prediction; (ii) position knowledge is perfect during prediction, but not during building the training database. In the latter case, (31)–(32) can still be used, though the covariance of the prediction location should be set to zero.

VI. APPLICATIONS OF CHANNEL GAIN PREDICTION

In this section, we first elaborate on different kinds of applications, allowing to incorporate the channel prediction framework from Sec. V naturally. Then, we study in detail the problem of maximizing network communication quality, as introduced in Sec. III, with the help of cGP and uGP.

A. Channel Gain Prediction for Network Processing

The availability of the channel gain prediction framework presented in Sec. V has direct application in proactive resource allocation for mobile users not only to improve the users' quality of service, but also to increase the overall network throughput [3], [59]. In 5G networks, channel gain prediction can be used in resource allocation at different layers of the protocol stack with the benefit of reducing latency and/or overheads (see [60] for specific examples). Further applications involve cooperative spectrum sensing [61], where uGP exploits location uncertainty of the recorded measurement and the test locations, building of radio-maps in a distributed way [62], and for optimal sensor placement [30] to collect channel measurements (c.f. Sec. I).

B. Maximizing Network Communication Quality

We now revisit problem (6). The objective function of (6) can be expanded as

$$\sum_{e \in E} \mathbb{E}_{\gamma|\mathbf{u}_e} \{f(\gamma(\mathbf{u}_e))\} \tag{37}$$

$$= \sum_{e \in E} \int f(\gamma(\mathbf{u}_e)) p(\gamma(\mathbf{u}_e)|\mathcal{D}, \boldsymbol{\theta}, \mathbf{u}_e) \mathrm{d}\gamma(\mathbf{u}_e). \tag{38}$$

From Section V, we know that given a measurement database $\mathcal{D}$, where the measurements correspond to either known or uncertain locations, we can use uGP to (i) determine an estimate of the channel parameters $\boldsymbol{\theta}$, and (ii) predict the received power in a location $\mathbf{x}_*$ as having a Gaussian distribution with mean $\mathbb{E}\{P_{\mathrm{RX}}(\mathbf{x}_*)|\mathcal{D}, \boldsymbol{\theta}, \mathbf{x}_*\}$ and variance $\mathbb{V}\{P_{\mathrm{RX}}(\mathbf{x}_*)|\mathcal{D}, \boldsymbol{\theta}, \mathbf{x}_*\}$. Moreover, even when the location in which we want to predict the received power is uncertain, we can determine $\mathbb{E}\{P_{\mathrm{RX}}(\mathbf{u}_*)|\mathcal{D}, \boldsymbol{\theta}, \mathbf{u}_*\}$ and $\mathbb{V}\{P_{\mathrm{RX}}(\mathbf{u}_*)|\mathcal{D}, \boldsymbol{\theta}, \mathbf{u}_*\}$. In the specific case where measurements and prediction are related to known locations, uGP reverts to cGP. Thus, we can focus on the case where all locations are uncertain.

If uGP predicts that the received power in dBm $P_{\mathrm{RX}}(\mathbf{u}_e) \sim \mathcal{N}(\mu_e, \sigma_e^2)$, then the SNR in the linear domain $\gamma(\mathbf{u}_e)$ can be expressed as

$$\gamma(\mathbf{u}_e) = \exp(-10\kappa \log_{10}(\sigma_n^2)) \exp(\kappa P_{\mathrm{RX}}(\mathbf{u}_e)), \tag{39}$$

where $\sigma_n^2 = N_0 W$ is the noise power, and $\kappa = \ln 10/10$. Hence, $\gamma(\mathbf{u}_e)$ has a log-normal distribution:

$$\gamma(\mathbf{u}_e) \sim \ln \mathcal{N}(\kappa\mu_e - 10\kappa \log_{10}(\sigma_n^2), \kappa^2 \sigma_e^2). \tag{40}$$

This means that, by converting to the linear domain and accounting for the noise power, we have a distribution of $\gamma(\mathbf{u}_e)$ in the form of a log-normal distribution. We consider again the three examples of $f(\cdot)$ introduced in Section III:

- *Case 1: $f(\cdot)$ depends linearly on the SNR.* If $P_{\mathrm{RX}}(\mathbf{u}_e) \sim \mathcal{N}(\mu_e, \sigma_e^2)$, then

$$\mathbb{E}_{\gamma|\mathbf{u}_e} \{\gamma(\mathbf{u}_e)\} \propto \exp\left(\kappa\mu_e + \kappa^2 \sigma_e^2/2\right), \tag{41}$$

- *Case 2: $f(\cdot)$ depends on the logarithm of the SNR.* Following [53, Eq. (18)], introducing $m_e = \kappa \left(b_e[\mathrm{dB}] + \mu_e - 10 \log_{10}(\sigma_n^2)\right)$ and

$$\mathbb{E}_{\gamma|\mathbf{u}_e} \{\ln\left(1 + b_e \gamma(\mathbf{u}_e)\right)\} \tag{42}$$

$$\approx \ln\left(2 \cosh\left(\frac{m_e}{2}\right)\right) + \frac{m_e}{2} + \frac{1}{2}\frac{\kappa\sigma_e\eta_0}{\sqrt{2}} \cosh^{-\eta_1}\left(\frac{m_e}{2\eta_2}\right),$$

in which η_0, η_1, and η_2 are polynomials in σ_e. For high SNR, $\mathbb{E}_{\gamma|\mathbf{u}_e} \{\ln\left(1 + b_e \gamma(\mathbf{u}_e)\right)\} \approx m_e$.

- *Case 3: $f(\cdot)$ depends on the exponential of the SNR.* Now, $f(\gamma(\mathbf{u}_e)) = a_e + b_e \exp(-c_e\gamma(\mathbf{u}_e))$. Due the linearity of expectation, we can focus on $f(\gamma(\mathbf{u}_e)) = \exp(-c_e\gamma(\mathbf{u}_e))$. We note that

$$\mathbb{E}_{\gamma|\mathbf{u}_e} \{\exp(-c_e\gamma(\mathbf{u}_e))\} = \mathcal{L}_\Gamma(c_e), \tag{43}$$

where $\mathcal{L}_\Gamma(\cdot)$ is the Laplace transform of the distribution of the random variable $\gamma(\mathbf{u}_e)$. Since $\gamma(\mathbf{u}_e)$ is a log-normal random variable, no closed-form expression of the Laplace transform is available. Using the approximation from [63], we find that

$$\mathbb{E}_{\gamma|\mathbf{u}_e} \{\exp(-c_e\gamma(\mathbf{u}_e))\} \tag{44}$$

$$\approx \frac{1}{\sqrt{1 + \omega(\zeta)}} \exp\left(-\frac{1}{2\kappa^2\sigma_e^2}(\omega(\zeta))^2 - \frac{1}{\kappa^2\sigma_e^2}\omega(\zeta)\right), \tag{45}$$

where $\omega(\cdot)$ is the Lambert W-function, which is defined as the solution of the equation $\omega(x)e^{\omega(x)} = x$, and

$$\zeta = c_e\kappa^2\sigma_e^2 \exp(\kappa\mu_e - 10\kappa \log_{10}(\sigma_n^2)). \tag{46}$$

In summary, for each choice of $f(\cdot)$ in (6), the solution obtained by uGP can be used to evaluate the objective function, either exactly or approximately.

VII. RESULTS

In this section, we present results for channel learning and prediction, as well as communication quality optimization, all in the presence of location uncertainty. To generate the channels, we use the channel simulator presented in [37], which uses a sum-of-sinusoids approach to establish the spatial correlation of the underlying Gaussian process, fed with parameters from the indoor measurements.

Parameters: Unless specified otherwise, the synthetic channel measurements were generated with path-gain $L_0 = -10$ dBm, path loss exponent $\eta = 2$, shadowing decorrelation distance $d_c = 3$ m and standard deviation $\sigma_\Psi = 7$ dB. The RX noise standard deviation is $\sigma_n = 0.01$. The covariance function uses $\kappa = 1$ for the true field and for cGP, while uGP uses $\kappa = 2$.

A. Learning Under Location Uncertainty

We make use of the synthetic ad-hoc channel simulator to generate measurements within the workspace $\mathcal{W} \subset 30$ m $\times$ 30 m. The training database $\mathcal{D}$ consists of $N = 700$ measurements collected at locations $\mathbf{x}_i = [\mathbf{q}_{\mathrm{TX},i}^\mathrm{T}, \mathbf{q}_{\mathrm{RX},i}^\mathrm{T}]^\mathrm{T}$, where $\mathbf{q}_{\mathrm{TX},i} = [15 \text{ m}, 15 \text{ m}]^\mathrm{T}$ and $\mathbf{q}_{\mathrm{RX},i}$ is randomly distributed within $\mathcal{W}$ for $i = 1, \ldots, N$. Location uncertainty is introduced
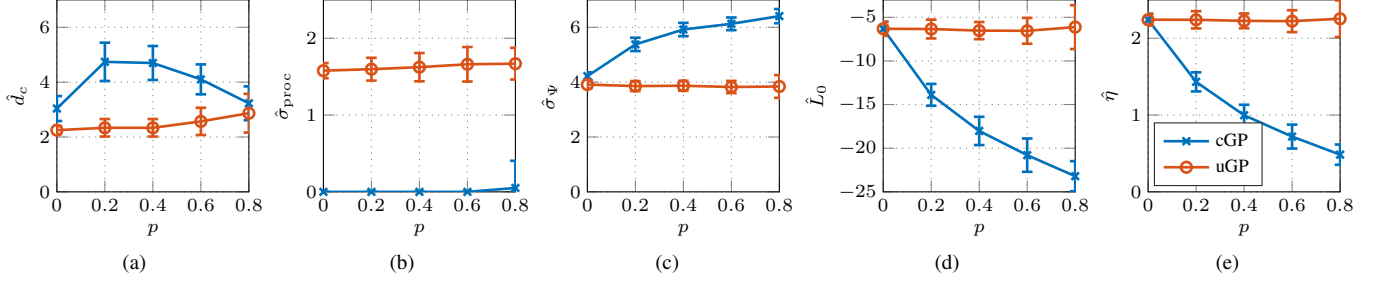
Fig. 4. Learning with location uncertainty: hyper-parameters of cGP and uGP method learned from synthetic measurement data for different fractions p of measurement data with high location uncertainty. The errorbars indicate one standard deviation confidence interval. Channel parameters of true field: $d_c = 3$ m, $\sigma_{\mathrm{proc}} = 0$, $\sigma_\Psi = 7$ dB, $L_0 = -10$ dBm, $\eta = 2$.

as follows: a fraction $p \in [0, 0.8]$ of the locations has high location uncertainty, corresponding to a location standard deviation of 10 meters in all directions, whereas the remaining locations have no location uncertainty. cGP has only access to the estimated locations (i.e., $\boldsymbol{\mu}_i$), while uGP has access to the distributions of the locations (i.e., $\mathbf{u}_i$). Note that for uGP, we omit step 4 of the learning procedure used to solve (35). All results are averaged over 50 Monte Carlo runs.

In Fig. 4, the learned hyper-parameters for cGP and uGP are plotted together with one standard deviation confidence interval for different fractions p of measurements with high location uncertainty. When there is no location uncertainty in the training database ($p = 0$), the estimate for L_0 and η is the same for cGP and uGP, since the weighted least squares estimation in uGP falls back to the least squares estimation of cGP. When $p > 0$, the estimates $\hat{L}_0$ and $\hat{\eta}$ decrease significantly with increasing p in the case of cGP. This means the estimation of the deterministic path-loss parameters fails. The learned mean function (11) basically becomes zero. In contrast to this, uGP can easily cope with location uncertainty of the training samples. The estimated parameters for L_0 and η remain constant. For larger values of p, the variance of the estimates increases.

When we inspect the estimated kernel parameters, cGP operates on a non-zero mean field, due to the incorrect estimates of L_0 and η. cGP explains this field by considering it as slowly varying, leading to an increase in the estimate of σ_Ψ. In contrast, uGP, leads to a more desired behavior: the estimates remain more or less constant, irrespective of p, though the variance of the estimates tends to increase again with p (since fewer good measurements are available).

In summary, cGP and uGP explain the measurement in completely different ways: whereas uGP can account for both the mean and covariance functions, cGP essentially ignores the mean function, leading to a larger spread in the estimated parameters.

B. Prediction Under Location Uncertainty

Next, we study how location uncertainty at the test location $\mathbf{x}_* = [\mathbf{q}_{\mathrm{TX}}^\mathrm{T}, \mathbf{q}_{\mathrm{RX}}^\mathrm{T}]^\mathrm{T}$ influences the predicted mean RX power. We quantify the mean RX power by

$$\bar{P}_{\mathrm{RX}} \triangleq \mathbb{E}_{\mathbf{x}_*} \{P_{\mathrm{RX}}(\mathbf{x}_*)\} = \int P_{\mathrm{RX}}(\mathbf{x}_*) p(\mathbf{x}_*) d\mathbf{x}_*. \quad (47)$$

For the sake of clarity, we will only consider uncertainty in the receiver location $\mathbf{q}_{\mathrm{RX}}$. We predict $\bar{P}_{\mathrm{RX}}$ using (15) in the case of cGP and using (31) in the case of uGP. In the latter case, we predict $\bar{P}_{\mathrm{RX}}$ w.r.t. its location pdf $p(\mathbf{q}_{\mathrm{RX}})$. In the workspace $\mathcal{W} \subset 50$ m $\times$ 50 m we query the synthetic ad-hoc channel simulator to obtain $N = 700$ measurements, including reciprocal measurements, at RX locations placed on a grid in $\mathcal{W}$ yielding the training database $\mathcal{D}$. The training measurements have no location uncertainty and the estimated hyper-parameters correspond to the values in Fig. 4 for $p = 0$, for both cGP and uGP. For the prediction, the TX is placed at a fixed location $\mathbf{q}_{\mathrm{TX}} = [5 \text{ m}, 30 \text{ m}]^\mathrm{T}$, while the receiver moves over $\mathbf{q}_{\mathrm{RX}} = [30 \text{ m}, y]^\mathrm{T}$, $y \in [0 \text{ m}, 50 \text{ m}]$. The location uncertainty standard deviation σ_{RX} during prediction is set to 0 m for $y < 25$ m and to 10 m for $y \geq 25$ m.

In Fig. 5, the mean RX power $\bar{P}_{\mathrm{RX}}$ is plotted as a function of y. Additionally, the predicted mean and one standard deviation confidence interval of cGP using (15) and (16) is shown. We observe that the predicted mean closely follows $\bar{P}_{\mathrm{RX}}$ for $y < 25$ m. Furthermore, the true mean RX power is mostly inside the one standard deviation confidence interval. The log-likelihood of prediction (15) and true mean (47) with respect to the predicted variance (16) is -97.46. For $y \geq 25$ m, cGP is still confident about its prediction (15), but tends to be far off from the true mean (47) having a log-likelihood of -128.04. This is in contrast to a desirable behavior of any predictor, i.e., where the estimate follows the true value with a low standard deviation. Hence, cGP fails to give a reliable prediction for $\bar{P}_{\mathrm{RX}}$ in regimes with high location uncertainty. In Fig. 6, the same mean RX power $\bar{P}_{\mathrm{RX}}$ for different values of $\mathbf{q}_{\mathrm{RX}}$ is plot as in the previous case. Also shown are the uGP predicted mean and one standard deviation confidence interval using (31) and (32). We observe that uGP is able to predict the mean RX power equally well in the regime 0 m $\leq y < 25$ m. The log-likelihood of prediction (31) and true mean (47) with respect to the predicted variance (32) is -97.18. As soon as $y \geq 25$ m, the predicted mean RX power becomes much smoother and at the same time the confidence interval is increased. This combination leads to a robust prediction w.r.t. the predicted variance resulting in a higher log-likelihood of -120.20 compared to cGP.
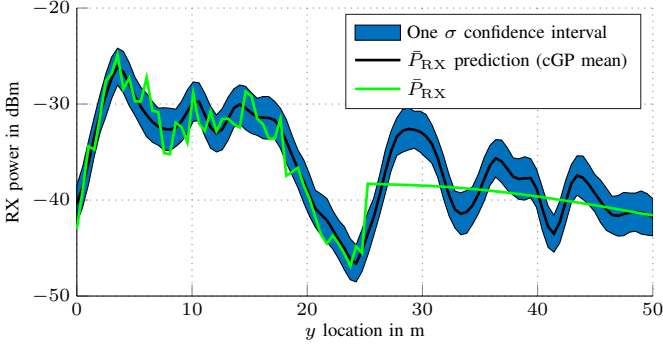
Fig. 5. Prediction using cGP: mean RX power $\bar{P}_{\mathrm{RX}}$ for different locations together with cGP prediction (mean and one standard deviation).
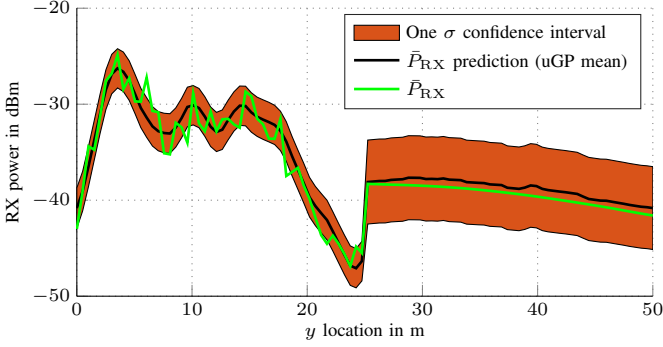

Fig. 6. Prediction using uGP: mean RX power $\bar{P}_{\mathrm{RX}}$ for different locations together with uGP prediction (mean and one standard deviation).

C. Application Example: Optimal Router Configuration Under Location Uncertainty

As an application, we consider the setup from [24], but with location uncertainty of the TX and RX agents in fading environments. In doing so, we seek to minimize the BER of data transmitted from a source agent until it reaches a destination agent over a wireless network with $L - 2$ intermediate agents, which act as relays (similar to the scenario in Fig. 1, where $L = 5$). Since the BER depends on the channel quality on each of the $L - 1$ links, we are interested in finding the optimal locations of the relay agents taking into account location uncertainty of the agents in the environment. The objective function we adopt is the probability of correct reception from agent 1 to agent L [24, eq. (23) and (25)]

$$J(\mathbf{X}) = \prod_{i=2}^{L} \left(1 - 0.2\mathbb{E}_{\gamma|\mathbf{x}_i}\left\{\exp(-c\gamma(\mathbf{x}_i))\right\}\right), \qquad (48)$$

where c is a known constant and the BER is defined as $\mathrm{BER} = 1 - J(\mathbf{X})$. Hence, in our context with location uncertainty, we will solve

$$\underset{\mathbf{U}\in\mathcal{U}}{\text{maximize}} \sum_{i=2}^{L} \ln\left(1 - 0.2\mathbb{E}_{\gamma|\mathbf{u}_i}\left\{\exp(-c\gamma(\mathbf{u}_i))\right\}\right), \qquad (49)$$

which is in the form studied in Section VI-B, Case 3.

We consider a workspace of $\mathcal{W} \subset 50\,\mathrm{m}\times50\,\mathrm{m}$ and place the source agent, denoted agent 1, at location $\mathbf{q}_1 = [5\,\mathrm{m}, 30\,\mathrm{m}]^{\mathrm{T}}$ and the destination agent, denoted agent L, at location $\mathbf{q}_L =$

$[45\,\mathrm{m}, 30\,\mathrm{m}]^{\mathrm{T}}$. Data communication from agent 1 to agent L is relayed via N_r relay agents. Such a communication network is outlined in Fig. 1. The number of relay agents considered is $N_{\mathrm{r}} = \{1, 2\}$. We assume both, cGP and uGP, have access to an associated measurement database $\mathcal{D}$, where the measurement locations are on a rectangular grid in $\mathcal{W}$, i.e., between all possible TX and RX location combinations, with spacing of $2.58\,\mathrm{m}$. Furthermore, we include the reciprocal channel measurements. We assume the measurement locations in the measurement database to have perfect location information. The used channel parameters match with the results of Fig. 4 for the case of no location uncertainty in the measurement database. We will investigate the effect of location uncertainty on channel prediction. Therefore, let us assume that whenever a relay agent $\mathbf{q}_i$ is placed in the upper half of $\mathcal{W}$, the agent will experience location uncertainty with standard deviation of $10\,\mathrm{m}$ per dimension.

We solve (49) via an exhaustive grid search and via a greedy search. The greedy search works as follows. First, we solve (49) with the help of a grid search for the case only one relay is used, i.e., $N_r = 1$ where the communication graph has edges from agent 1 to agent 2 and from agent 2 to agent L (c.f. Fig. 1). We then fix agent 2 to the computed optimal location and introduce a new relay agent 3. Similarly as before, (49) is solved, where in this case the communication graph has edges between agent 1 and 2, 2 and 3, and 3 and L. Note that now all locations except of relay agent 3 are known and hence, they are not optimization variables in (49). With the optimal location of agent 3, we can solve (49) again to find the new optimal location for agent 2 since the location of its link endpoints has changed. This process of iterating between the relays, while keeping the link endpoints location fixed, is repeated $N_{\mathrm{iter}} = 10$ times. The greedy search algorithm proceeds by adding more relays in this manner until N_r relay locations have been determined. Although suboptimal, the greedy search has the benefit that its computational complexity is linear w.r.t. the number of relay agents N_r. Alternatively, a global solution to (49) may be found using any global solver such as, for instance, simulated annealing [64], a genetic algorithm [65], or the cross-entropy method [66].

After solving (49), we aim to place the relays in the optimal locations (means of the optimal location distribution in the case of uGP), denoted by $\mathbf{q}_i$ for relays $i = 2,..,L-1$. Due to the (possibly) present location uncertainty at the optimal location $\mathbf{q}_i$, relay agent i aiming to traverse there may not arrive exactly at $\mathbf{q}_i$. For this reason, the actual location where the relay ends up becomes random and follows $\mathbf{z}_i \sim \mathcal{N}(\mathbf{q}_i, \sigma_i^2(\mathbf{q}_i)\mathbf{I}_2)$, where $\sigma_i(\mathbf{q}_i)$ represents the uncertainty in that location (i.e., either zero or $10\,\mathrm{m}$). While the BER itself is not random, the locations where we evaluate the BER are random (due to present location uncertainty). Hence, the achieved BER becomes a random variable for both cGP and uGP. In Fig. 7, we plot the cumulative distribution function (cdf) of the actual achieved BER, i.e., the BER evaluated at relay locations $\mathbf{z}_i$, for cGP and uGP using both, the exhaustive grid search and the greedy search method. For cGP and $N_r = 1$, the optimal relay location is in the part of the workspace with high location uncertainty, which leads to
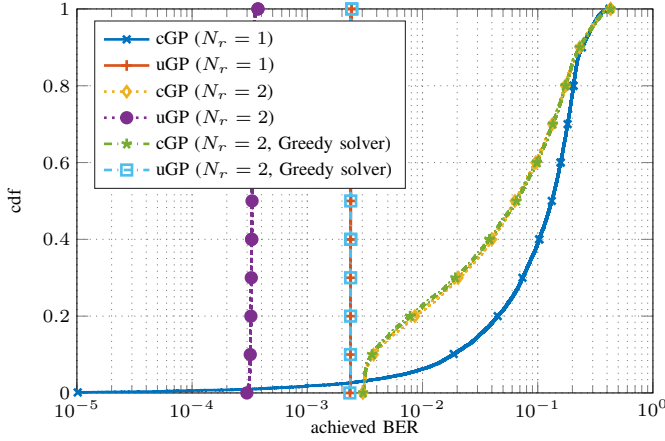
Fig. 7. The cdf of the achieved end-to-end BER is plot for multi-relay communication. Solving (49) determined the optimal relay locations, which involved the application of cGP and uGP.

large variations in the achieved BER over all realizations of the relay position $\mathbf{z}_i$. The average achieved BER is 0.13. For the case $N_r = 2$, the average achieved BER has reduced slightly to $9.6 \cdot 10^{-2}$, where the exhaustive grid search and the greedy search determined the same optimal relay locations. In Fig. 7, we observe large variations of the achieved BER for this case as well, since one of the optimal relay locations is in the part of the workspace with high location uncertainty. Due to the large variations of the achieved BER we can conclude that the use of cGP leads to unpredictable performance if agents need to operate in areas with high location uncertainty. In contrast, when using uGP, we observe that for both, $N_r = 1$ and $N_r = 2$, solutions with low location uncertainty are preferred, i.e., the cdf has a steep increase over the achieved BER. Moving from case $N_r = 1$ to $N_r = 2$ and using the greedy search yields no performance gain, whereas with an exhaustive search the average achieved BER is reduced to $3.3 \cdot 10^{-4}$ for all realizations of the relay positions of both relay agents. If uGP is used for channel prediction, which incorporates any present location uncertainty, we see a clear gain in terms of BER by using more relay agents for the case the exhaustive search is used to find the global minimum of (49). Hence, we conclude that considering location uncertainty of relay agents leads to a significantly lower achieved BER compared to methods ignoring location uncertainty.

VIII. CONCLUSIONS

We considered a communication relay placement problem for end-to-end communication quality maximization in a multi-agent system with location uncertainty. We developed a Gaussian process (GP) channel prediction framework, capable to model, learn, and predict the wireless channel. The developed GP framework works on the input space of location distributions, rather than the transmitter (TX) and receiver (RX) locations themselves, allowing to properly incorporate channel measurements recorded at TX–RX locations with heterogeneous location uncertainty. In doing so, we presented a novel learning approach and closed form expressions for the mean and variance of the predictive distribution of the received

power at any test TX–RX location pair. We observed that taking location uncertainty in channel prediction into account results in an end-to-end communication quality that is robust with respect to the variations of the channel and the location uncertainty of the involved agents.

APPENDIX A
PROOF OF THEOREM 1

Proof: Combining (8) with (23) yields

$$\mu_{\text{uGP}}(\mathbf{u}) = L_0 - 10\eta \mathbb{E}_{\mathbf{q}_{\text{TX}}, \mathbf{q}_{\text{RX}}} \{ \log_{10} \|\mathbf{q}_{\text{TX}} - \mathbf{q}_{\text{RX}}\|_2 \} \quad (50)$$

and we can now focus only on the part which depends on the expectation w.r.t. $\mathbf{q}_{\text{TX}}, \mathbf{q}_{\text{RX}}$. Define $\mathbf{w} = \mathbf{q}_{\text{TX}} - \mathbf{q}_{\text{RX}}$, where $\mathbf{w} \sim \mathcal{N}(\boldsymbol{\mu}, \sigma^2 \mathbf{I})$ with $\boldsymbol{\mu} = \boldsymbol{\mu}_{\text{TX}} - \boldsymbol{\mu}_{\text{RX}}$ with elements $\boldsymbol{\mu} = [\mu_1, \mu_2]^{\text{T}}$ and $\sigma^2 = \sigma_{\text{TX}}^2 + \sigma_{\text{RX}}^2$.[3] This translates $\mathbb{E}_{\mathbf{u}} \{ \log_{10} \|\mathbf{q}_{\text{TX}} - \mathbf{q}_{\text{RX}}\|_2 \}$ into the equivalent problem of finding

$$\mathbb{E}_{\mathbf{w}} \{ \log_{10} \|\mathbf{w}\|_2 \} = \frac{1}{\ln 10} \frac{1}{2} \mathbb{E}_{\mathbf{w}} \{ \ln \|\mathbf{w}\|_2^2 \}. \quad (51)$$

From [67, Appendix X, Lemma 10.1] we know

$$\mathbb{E}\{\ln V\} = g_m(s^2) \quad (52)$$

is non-central chi-square distributed with $2m$ degrees of freedom for $V = \sum_{j=1}^{m} |U_j + \mu_j|^2$, where $U_j \sim \mathbb{C}\mathcal{N}(0, 1)$, and μ_j are complex constants for $j = 1, 2, \ldots, m$. The parameter s^2 denotes the non-centrality parameter and $s^2 = \sum_{j=1}^{m} |\mu_j|^2$. The function $g_m(\cdot)$ is defined as

$$
\begin{aligned}
g_m(\xi) = {} & \ln \xi - E_i(-\xi) + \\
& \sum_{j=1}^{m-1} (-1)^j \left[e^{-\xi}(j-1)! - \frac{(m-1)!}{j(m-1-j)!} \right] \left(\frac{1}{\xi} \right)^j
\end{aligned}
$$

for $\xi > 0$ and $g_m(\xi) = \psi(m)$ for $\xi = 0$. Here, the parameter $m \in \mathbb{Z}^+$, the function $E_i(\cdot)$ is defined in (25), and $\psi(m)$ is the digamma function for integer m (sometimes also denoted Euler's psi function) given by

$$\psi(m) = -\gamma + \sum_{j=1}^{m-1} \frac{1}{j}, \quad (53)$$

where $\gamma \approx 0.577$ denotes Euler's constant. In the following, we rewrite $\mathbf{u}_{\text{TX}}$ and $\mathbf{u}_{\text{RX}}$ by complex normal distributed random variables with zero mean and unit variance to adapt the result above appropriately. For $X_1 \sim \mathcal{N}(\mu_1, \sigma^2)$ and $X_2 \sim \mathcal{N}(\mu_2, \sigma^2)$, we see

$$X_1^2 + X_2^2 = (\sigma U_1 + \mu_1)^2 + (\sigma U_2 + \mu_2)^2, \quad (54)$$

where $U_1, U_2 \sim \mathcal{N}(0, 1)$. Equivalently,

$$X_1^2 + X_2^2 = \|\sigma(U_1 + jU_2) + \mu_1 + j\mu_2\|_2^2, \quad (55)$$

where $j = \sqrt{-1}$. Let us introduce $U_* \sim \mathbb{C}\mathcal{N}(0, 1)$, where $U_* = \frac{1}{\sqrt{2}}(U_1 + jU_2)$. Then

$$X_1^2 + X_2^2 = 2\sigma^2 \|U_* + \mu_*\|_2^2, \quad (56)$$

[3]Note, TX and RX locations are assumed to be independent of each other, since there exists only a wireless communication link between different agents.

where $\mu_* = \frac{\mu_1 + j\mu_2}{\sigma\sqrt{2}}$. Note above, a factor $2\sigma^2$ is present. Define $V_* = 2\sigma^2|U_* + \mu_*|^2$. Hence,

$$\mathbb{E}\{\ln V_*\} = \ln 2\sigma^2 + \mathbb{E}\{\ln V\} \tag{57}$$

with $V = |U_* + \mu_*|^2$. Then, (52) from above can be used. For the special case $m = 1$, the random variable V is said to have a squared Rician distribution, where

$$\mathbb{E}\{\ln V\} = \mathbb{E}\{\ln|U_* + \mu_*|^2\} = \ln(|\mu_*|^2) - E_i(-|\mu_*|^2). \tag{58}$$

To obtain (24), we replace the expectation in (51) by the closed-form expression (58) and plug it back into (50). ∎

REFERENCES

[1] Y. Zeng, R. Zhang, and T. J. Lim, "Wireless Communications with Unmanned Aerial Vehicles: Opportunities and Challenges," *IEEE Communications Magazine*, vol. 54, no. 5, pp. 36–42, May 2016.

[2] M. A. Hsieh, A. Cowley, V. Kumar, and C. J. Taylor, "Maintaining Network Connectivity and Performance in Robot Teams," *Journal of Field Robotics*, vol. 25, no. 1-2, pp. 111–131, 2008.

[3] L. S. Muppirisetty, J. Tadrous, A. Eryilmaz, and H. Wymeersch, "On Proactive Caching with Demand and Channel Uncertainties," in *53rd Annual Allerton Conference on Communication, Control, and Computing*, Sept 2015, pp. 1174–1181.

[4] H. Abou-Zeid and H. S. Hassanein, "Predictive Green Wireless Access: Exploiting Mobility and Application Information," *Wireless Communications, IEEE*, vol. 20, no. 5, pp. 92–99, 2013.

[5] M. Alsabaan, W. Alasmary, A. Albasir, and K. Naik, "Vehicular Networks for a Greener Environment: A Survey," *Communications Surveys & Tutorials, IEEE*, vol. 15, no. 3, pp. 1372–1388, 2013.

[6] E. Steinmetz, R. Hult, G. Rodrigues de Campos, M. Wildemeersch, P. Falcone, and H. Wymeersch, "Communication analysis for centralized intersection crossing coordination," in *11th International Symposium on Wireless Communications Systems*. IEEE, 2014, pp. 813–818.

[7] H. Wymeersch, G. R. de Campos, P. Falcone, L. Svensson, and E. G. Ström, "Challenges for Cooperative ITS: Improving Road Safety Through the Integration of Wireless Communications, Control, and Positioning," in *International Conference on Computing, Networking and Communications*. IEEE, 2015, pp. 573–578.

[8] B. J. Julian, M. Angermann, M. Schwager, and D. Rus, "Distributed robotic sensor networks: An information-theoretic approach," *The International Journal of Robotics Research*, vol. 31, no. 10, pp. 1134–1154, 2012.

[9] S. Waharte and N. Trigoni, "Supporting Search and Rescue Operations with UAVs," in *International Conference on Emerging Security Technologies*, Sept 2010, pp. 142–147.

[10] G. Karagiannis, O. Altintas, E. Ekici, G. Heijenk, B. Jarupan, K. Lin, and T. Weil, "Vehicular Networking: A Survey and Tutorial on Requirements, Architectures, Challenges, Standards and Solutions," *IEEE Communications Surveys Tutorials*, vol. 13, no. 4, pp. 584–616, 2011.

[11] A. A. Zaidi, B. Kulcsár, and H. Wymeersch, "Traffic-adaptive Signal Control and Vehicle Routing Using a Decentralized Back-pressure Method," in *European Control Conference*, July 2015, pp. 3029–3034.

[12] D. P. Spanos and R. M. Murray, "Motion Planning with Wireless Network Constraints," in *Proceedings of the American control conference*, vol. 1, 2005, pp. 87–92.

[13] M. M. Zavlanos and G. J. Pappas, "Distributed Connectivity Control of Mobile Networks," *IEEE Transactions on Robotics*, vol. 24, no. 6, pp. 1416–1428, 2008.

[14] M. M. Zavlanos, M. B. Egerstedt, and G. J. Pappas, "Graph-Theoretic Connectivity Control of Mobile Robot Networks," *Proceedings of the IEEE*, vol. 99, no. 9, pp. 1525–1540, 2011.

[15] A. Simonetto, T. Keviczky, and R. Babuska, "Constrained distributed algebraic connectivity maximization in robotic networks," *Automatica*, vol. 49, no. 5, pp. 1348–1357, 2013.

[16] J. Cortés, S. Martínez, and F. Bullo, "Spatially-distributed coverage optimization and control with limited-range interactions," *ESAIM: Control, Optimisation and Calculus of Variations*, vol. 11, no. 04, pp. 691–719, 2005.

[17] N. M. M. De Abreu, "Old and new results on algebraic connectivity of graphs," *Linear algebra and its applications*, vol. 423, no. 1, pp. 53–73, 2007.

[18] N. Michael, M. M. Zavlanos, V. Kumar, and G. J. Pappas, "Maintaining Connectivity in Mobile Robot Networks," in *Experimental Robotics*. Springer, 2009, pp. 117–126.

[19] M. M. Zavlanos, A. Ribeiro, and G. J. Pappas, "Network Integrity in Mobile Robotic Networks," *IEEE Transactions on Automatic Control*, vol. 58, no. 1, pp. 3–18, Jan 2013.

[20] ——, "Mobility & Routing Control in Networks of Robots," in *49th IEEE Conference on Decision and Control (CDC)*, Dec 2010, pp. 7545–7550.

[21] ——, "A Framework for Integrating Mobility and Routing in Mobile Communication Networks," in *2011 Conference Record of the Forty Fifth Asilomar Conference on Signals, Systems and Computers (ASILOMAR)*, Nov 2011, pp. 1461–1465.

[22] A. Ribeiro, N. D. Sidiropoulos, and G. B. Giannakis, "Optimal Distributed Stochastic Routing Algorithms for Wireless Multihop Networks," *IEEE Transactions on Wireless Communications*, vol. 7, no. 11, pp. 4261–4272, Nov 2008.

[23] J. Fink, "Communication for teams of networked robots," Ph.D. dissertation, University of Pennsylvania, 2011.

[24] Y. Yan and Y. Mostofi, "Robotic Router Formation in Realistic Communication Environments," *IEEE Transactions on Robotics*, vol. 28, no. 4, pp. 810–827, 2012.

[25] J. Cortés, S. Martínez, T. Karatas, and F. Bullo, "Coverage Control for Mobile Sensing Networks," *IEEE Transactions on Robotics and Automation*, vol. 20, no. 2, pp. 243–255, Apr 2004.

[26] S. Martínez and F. Bullo, "Optimal sensor placement and motion coordination for target tracking," *Automatica*, vol. 42, no. 4, pp. 661–668, 2006.

[27] K. M. Lynch, I. B. Schwartz, P. Yang, and R. A. Freeman, "Decentralized Environmental Modeling by Mobile Sensor Networks," *IEEE Transactions on Robotics*, vol. 24, no. 3, pp. 710–724, Jun 2008.

[28] H. M. La, W. Sheng, and J. Chen, "Cooperative and Active Sensing in Mobile Sensor Networks for Scalar Field Mapping," *IEEE Transactions on Systems, Man, and Cybernetics: Systems*, vol. 45, no. 1, pp. 1–12, Jan 2015.

[29] F. Meyer, H. Wymeersch, M. Fröhle, and F. Hlawatsch, "Distributed Estimation With Information-Seeking Control in Agent Networks," *IEEE Journal on Selected Areas in Communications*, vol. 33, no. 11, pp. 2439–2456, Nov 2015.

[30] A. Krause, A. Singh, and C. Guestrin, "Near-optimal sensor placements in gaussian processes: Theory, efficient algorithms and empirical studies," *Journal of Machine Learning Research*, vol. 9, no. Feb, pp. 235–284, 2008.

[31] N. Jalden, "Analysis and Modelling of Joint Channel Properties from Multi-site, Multi-Antenna Radio Measurements," Ph.D. dissertation, KTH, Signal Processing, 2010.

[32] A. Böttcher, P. Vary, C. Schneider, and R. S. Thomä, "De-Correlation Distance of the Large Scale Parameters in an Urban Macro Cell Scenario," in *6th European Conference on Antennas and Propagation (EUCAP)*, 2012, pp. 1417–1421.

[33] Z. Li, R. Wang, and A. F. Molisch, "Shadowing in urban environments with microcellular or peer-to-peer links," in *6th European Conference on Antennas and Propagation*. IEEE, 2012, pp. 44–48.

[34] N. Jalden, P. Zetterberg, B. Ottersten, A. Hong, and R. Thomä, "Correlation Properties of Large Scale Fading Based on Indoor Measurements," in *IEEE Wireless Communications and Networking Conference*, March 2007, pp. 1894–1899.

[35] S. Szyszkowicz, H. Yanikomeroglu, and J. Thompson, "On the Feasibility of Wireless Shadowing Correlation Models," *IEEE Transactions on Vehicular Technology*, vol. 59, no. 9, pp. 4222–4236, 2010.

[36] M. Gudmundson, "Correlation model for shadow fading in mobile radio systems," *Electronics Letters*, vol. 27, no. 23, pp. 2145–2146, 1991.

[37] Z. Wang, E. K. Tameh, and A. R. Nix, "Joint Shadowing Process in Urban Peer-to-Peer Radio Channels," *IEEE Transactions on Vehicular Technology*, vol. 57, no. 1, pp. 52–64, 2008.

[38] P. Agrawal and N. Patwari, "Correlated Link Shadow Fading in Multi-Hop Wireless Networks," *IEEE Transactions on Wireless Communications*, vol. 8, no. 8, pp. 4024–4036, 2009.

[39] N. Patwari and P. Agrawal, "Effects of correlated shadowing: Connectivity, localization, and RF tomography," in *International Conference on Information Processing in Sensor Networks*. IEEE, 2008, pp. 82–93.

[40] ——, "NeSh: A joint shadowing model for links in a multi-hop network," in *IEEE International Conference on Acoustics, Speech and Signal Processing*. IEEE, 2008, pp. 2873–2876.

[41] M. Malmirchegini and Y. Mostofi, "On the Spatial Predictability of Communication Channels," *IEEE Transactions on Wireless Communications*, vol. 11, no. 3, pp. 964–978, 2012.

[42] K. V. Mardia, C. Goodall, E. J. Redfern, and F. J. Alonso, "The Kriged Kalman filter," *Test*, vol. 7, no. 2, pp. 217–282, 1998.

[43] J. Cortés, "Distributed Kriged Kalman Filter for Spatial Estimation," *IEEE Transactions on Automatic Control*, vol. 54, no. 12, pp. 2816–2827, Dec 2009.

[44] E. Dall'Anese, S. J. Kim, and G. B. Giannakis, "Channel Gain Map Tracking via Distributed Kriging," *IEEE Transactions on Vehicular Technology*, vol. 60, no. 3, pp. 1205–1211, Mar 2011.

[45] J. L. Ny and G. J. Pappas, "On Trajectory Optimization for Active Sensing in Gaussian Process Models," in *Proceedings of the 48h IEEE Conference on Decision and Control (CDC) held jointly with 2009 28th Chinese Control Conference*, Dec 2009, pp. 6286–6292.

[46] Y. Yan and Y. Mostofi, "Impact of Localization Errors on Wireless Channel Prediction in Mobile Robotic Networks," in *IEEE Globecom, Workshop on Wireless Networking for Unmanned Autonomous Vehicles*, 2013, pp. 1374–1379.

[47] M. Jadaliha, Y. Xu, J. Choi, N. S. Johnson, and W. Li, "Gaussian Process Regression for Sensor Networks Under Localization Uncertainty," *Signal Processing, IEEE Transactions on*, vol. 61, no. 2, pp. 223–237, 2013.

[48] L. S. Muppirisetty, T. Svensson, and H. Wymeersch, "Spatial Wireless Channel Prediction under Location Uncertainty," *IEEE Transactions on Wireless Communications*, vol. 15, no. 2, pp. 1031–1044, 2016.

[49] A. Girard, "Approximate Methods for Propagation of Uncertainty with Gaussian Process Models," Ph.D. dissertation, University of Glasgow, 2004.

[50] P. Dallaire, C. Besse, and B. Chaib-draa, "An approximate inference with Gaussian process to latent functions from uncertain data," *Neurocomputing*, vol. 74, no. 11, pp. 1945–1955, 2011.

[51] M. Fröhle, L. S. Muppirisetty, and H. Wymeersch, "Channel Gain Prediction for Multi-Agent Networks in the Presence of Location Uncertainty," in *IEEE International Conference on Acoustics, Speech and Signal Processing*, March 2016, pp. 3911–3915.

[52] S. Choudhury and J. D. Gibson, "Ergodic capacity, outage capacity, and information transmission over rayleigh fading channels," in *Proceedings of the Information Theory and Applications Workshop*, 2007.

[53] F. Heliot, X. Chu, R. Hoshyar, and R. Tafazolli, "An Accurate Closed-Form Approximation of the Ergodic Capacity over Log-Normal Fading Channels," in *IEEE 19th International Symposium on Personal, Indoor and Mobile Radio Communications*, 2008, pp. 1–5.

[54] A. Goldsmith, *Wireless Communications*. Cambridge University Press, 2005.

[55] G. L. Stüber, *Principles of Mobile Communication*. Springer Science & Business Media, 2011.

[56] D. Simon, *Optimal state estimation: Kalman, H infinity, and nonlinear approaches*. John Wiley & Sons, 2006.

[57] C. E. Rasmussen and C. K. I. Williams, *Gaussian processes for machine learning*. MIT Press, 2006.

[58] C. M. Bishop, *Pattern Recognition and Machine Learning*. Springer, 2006.

[59] L. S. Muppirisetty, S. Yiu, and H. Wymeersch, "LAPRA: Location-Aware Proactive Resource Allocation," in *2016 IEEE Global Communications Conference (GLOBECOM)*, Dec 2016, pp. 1–6.

[60] R. D. Taranto, S. Muppirisetty, R. Raulefs, D. Slock, T. Svensson, and H. Wymeersch, "Location-Aware Communications for 5G Networks: How location information can improve scalability, latency, and robustness of 5G," *IEEE Signal Processing Magazine*, vol. 31, no. 6, pp. 102–112, Nov 2014.

[61] I. Nevat, G. W. Peters, and I. B. Collings, "Location-aware Cooperative Spectrum Sensing via Gaussian Processes," in *2012 Australian Communications Theory Workshop (AusCTW)*, Jan 2012, pp. 19–24.

[62] V.-P. Chowdappa, M. Fröhle, H. Wymeersch, and C. Botella, "Distributed Channel Gain Prediction for Multi-Agent Systems," in *IEEE International Conference on Communications (ICC)*, May 2017, pp. 1–6.

[63] S. Asmussen, J. L. Jensen, and L. Rojas-Nandayapa, "On the Laplace Transform of the Lognormal Distribution," *Methodology and Computing in Applied Probability*, vol. 18, no. 2, pp. 441–458, 2014.

[64] S. Kirkpatrick, C. D. Gelatt, and M. P. Vecchi, "Optimization by Simulated Annealing," *Science*, vol. 220, no. 4598, pp. 671–680, 1983.

[65] K. Sastry, D. E. Goldberg, and G. Kendall, "Genetic Algorithms," in *Search methodologies*. Springer, 2014, pp. 93–117.

[66] P.-T. de Boer, D. P. Kroese, S. Mannor, and R. Y. Rubinstein, "A Tutorial on the Cross-Entropy Method," *Annals of Operations Research*, vol. 134, no. 1, pp. 19–67, 2005.

[67] A. Lapidoth and S. M. Moser, "Capacity Bounds Via Duality With Applications to Multiple-Antenna Systems on Flat-Fading Channels," *IEEE Transactions on Information Theory*, vol. 49, no. 10, pp. 2426–2467, 2003.

Markus Fröhle (S11) received the B.Sc. and M.Sc. degrees in Telematics from Graz University of Technology, Graz, Austria, in 2009 and 2012, respectively. He is currently working towards the Ph.D. degree in electrical engineering with the Department of Electrical Engineering, Chalmers University of Technology, Gothenburg, Sweden. From 2012 to 2013, he was a Research Assistant with the Signal Processing and Speech Communication Laboratory, Graz University of Technology. His current research interests include signal processing for wireless multi-agent systems, and localization and tracking.

Themistoklis Charalambous (M10) received the B.A. and M.Eng. degrees in electrical and information sciences from Cambridge University, Cambridge, U.K., in 2005. He received the Ph.D. degree in the Control Laboratory, of the Engineering Department, Cambridge University in 2010. He worked as a research associate at Imperial College London, as a Visiting Lecturer at the Department of Electrical and Computer Engineering, University of Cyprus, and as a post-doctoral researcher at the Automatic Control Lab of the School of Electrical Engineering at the Royal Institute of Technology (KTH) and at the Department of Electrical Engineering at Chalmers University of Technology. He is currently an Assistant Professor at the Department of Electrical Engineering and Automation, School of Electrical Engineering, Aalto University. His research involves distributed coordination and control, distributed decision making, and control to various resource allocation problems in complex and networked systems.
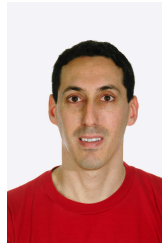
Ido Nevat received the B.Sc. degree in electrical engineering from the Technion-Israel Institute of Technology, Haifa, Israel in 1998 and the Ph.D. degree in Electrical Engineering from the University of NSW, Sydney, Australia, in 2010. Between 2010-2013 he was a postdoctoral research fellow with the Wireless and Networking Technologies Laboratory at CSIRO, Australia. Between 2013-2016 he was a scientist at the Institute for Infocomm Research (I2R), Singapore. He is now a team leader at TUMCREATE in Singapore. His main areas of interests include statistical signal processing, machine learning and Bayesian statistics.
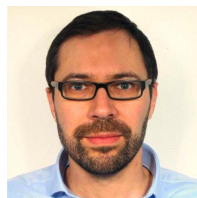
Henk Wymeersch (S01, M05) obtained the Ph.D. Degree in Electrical Engineering/Applied Sciences in 2005 from Ghent University, Belgium. He is currently a Professor of Communication Systems with the Department of Electrical Engineering at Chalmers University of Technology, Sweden. Prior to joining Chalmers, he was a postdoctoral researcher from 2005 until 2009 with the Laboratory for Information and Decision Systems at the Massachusetts Institute of Technology. Prof. Wymeersch served as Associate Editor for IEEE Communication Letters (2009-2013), IEEE Transactions on Wireless Communications (since 2013), and IEEE Transactions on Communications (since 2016). His current research interests include cooperative systems and intelligent transportation.